DISSERTATION REPORT

ON

CHARACTERIZATION OF BST BASED VARACTOR FOR PHASE SHIFTER APPLICATIONS

Submitted in partial fulfillment of the requirements for the award of degree of

MASTER OF TECHNOLOGY

In

Solid State Electronic Materials

Submitted By

ANIL KUMAR YADAVA

DEPARTMENT OF PHYSICS

INDIAN INSTITUTE OF TECHNOLOGY ROORKEE

INDIA (247667)

CANDIDATE’S DECLARATION

I hereby declare that the work, which is being presented in the project entitled, ***“ Characterization of BST Based Varactor for Phase Shifter Applications ”***, submitted in the partial fulfillment of the requirements for the award of degree of ***Master of Technology with specialization in Solid State Electronic Materials***, submitted in the Department of Physics, ***Indian Institute of Technology Roorkee, Roorkee (India)***, is an authentic record of my own work carried out from December, 2012 to June, 2013 under the supervision of **Professor R. Nath**, Department of Physics, Indian Institute of Technology, Roorkee.

I have not submitted the matter embodied in this project for the award of any other degree or diploma.

Date: - June-2013

Place: Roorkee (**Anil Kumar Yadava**)

CERTIFICATE

This is to certify that the statement made by the candidate is correct to the best of my knowledge and belief.

Date: - June-2013 **Professor R. Nath**

Place: Roorkee Department of Physics IIT, Roorkee

ACKNOWLEDGEMENTS

My special thanks to **Professor R. Nath**, my supervisor, for providing the time and equipment necessary for the work contained herein, and for directing this report and bringing it to its conclusion with patience and expertise.

I would also like to express my appreciation to **Dr. N.P.Pathak,** Associate Professor Department of Electronics and Communication Engineering, IIT Roorkee and **Dr. G.D.Varma,** Associate Professor Department of Physics, IIT Roorkee, have offered the use of test equipments and other resources without which this work could not have been completed in the same time table.

I thank **Mr. Rajaram, Mr. S.K.Gaur** for their valuable support and time to time guidance in technical issues, which was instrumental in making this dissertation work a success.

I also give special thanks to Research Scholars **A. V. Reddy sir**, Ferroelectric Materials and Devices Research Laboratory, Department of Physics and **Vivek Sharma sir,** Radio Frequency Integrated Circuits Research Laboratory, Department of Electronics & Computer Engineering, who shared his ideas and new concepts on this work and fabricates the devices, which helped to test these devices.

I am very grateful for the support of my parents, my brothers and sisters and Friends who always gave me spiritual support and encouragement to accomplish this task. Above all God must be praised!

ABSTRACT

The work presented here is on pure BST and Mg doped BST thin film. The fabrication of planer capacitor was done using sol-gel based spin coating technique on an n-type Si (100) substrate. High-quality thin films with uniform composition and well-developed dense crystalline structure with uniform grain size distribution were successfully produced. The main purpose of this work is to enhance the tunability as compared to conventional thin film materials while retaining the high voltage bias capability and higher phase shift at microwave frequencies.

The C –V characterization were studied for fabrication and design of BST varactor phase shifter. The BST thin films showed good dielectric properties. The phase shifter device based on coupled microstrip line structure was fabricated and design.

The $Ba_xSr_{1-x}TiO_3$ (x=0.5) thin films had paraelectric nature and loss tangent values at zero bias and f= 1 MHz were found to be 0.7 and 0.32 for undoped Mg doped BST film respectively. The leakage current density at 40 kV/cm was found to be .08A/cm^{2}in case of undoped BST and 0.0005A/cm^{2}for Mg doped BST films. It was found that C-V curve showed nonlinear dependence on applied field, thickness and annealed temperature. The tunability30% and 42% were observed for pure and Mg doped BST films respectively. However the phase shift of ~39^0 for BST and ~34^0 for the Mg doped BST were observed at 2.9GHz.

Table of Continents

Candidate's Declaration **i**

Certificate **i**

Acknowledgements **ii**

Abstract **iii**

Table of contents **iv**

CHAPTER - 1

INTRODUCTION **1**

1.1 Motivation and Background 1

1.2 An overview of tunable microwave devices 3

1.2.1 Review of non ferroelectric Technologies 4

1.2.2 Ferroelectric Technology 5

1.3 Dielectric properties of ferroelectric thin films 6

1.3.1 Ferroelectric thin film varactors 9

1.3.2 Basic structure of varactors 9

1.4 Barium strontium titanate ferroelectric thin films 10

1.5 Outline of this dissertation 11

CHAPTER – 2

FABRICATION AND MICROWAVE CHARACTERIZATION FERROELECTRIC THIN FILMS **12**

2.1 Fabrication of ferroelectric thin films 12

2.1.1 Chemical solution deposition of BST undoped and doped thin film 12

2.2 BST thin film characterization 16

2.2.1 Structural characterization 16

2.2.2 Electrical characterization 18

2.3 Microwave measurement techniques for ferroelectric thin films 21

2.3.1 Lumped capacitance measurement method 21

CHAPTER – 3

COUPLED MICROSTRIP LINE FERROELECTRIC THIN FILM VARACTOR PHASESHIFTERS **23**

3.1 Properties of coupled microstrip line 23

3.2 Phase shifter design 27

3.2.1 Calculation of phase shift and tunability 27

3.3 Fabrication of phase shifter 30

CHAPTER – 4

MEASUREMENT RESULTS AND DISCUSSION **31**

CHAPTER – 5

CONCLUSION AND FUTURE SCOPE **47**

References **48**

CHAPTER-1

INTRODUCTION

1.1 Motivation and Background

In the modern era, radio frequency (RF) and microwave engineering is an exciting and dynamic field due to its importance have in both commercial and military communication and radar systems, There has been explosive growth of commercial wireless markets and the interdependency between recent advances in modern electronic device technology. Which lead to the widespread use of RF/ microwave integrated circuit (IC) technology along with device miniaturization. This led to the development of RF and microwave circuit components whose dimensions are much smaller than their wavelength used. The miniaturization, reliability, ease of assembly and compactness of IC fabrication technology are the factors that tarmac the way for embedding these components directly into the substrates. In recent years, there has been fast growing demand for electrically tunable RF and microwave devices in wireless communications (cellular, Personal Data Assistants, IMT 2000, wireless LAN), digital electronics, Global Positioning Systems, modern radar system and mobile communication systems. The high dielectric nonlinearity (i.e. the strong dependence of dielectric constant on applied electric field) of ferroelectric materials with perovskite structure has made them promising candidates for these applications. The application of ferroelectric materials in electrically tunable RF and microwave devices was first introduced in the 1960's [1-4]. However, real applications of ferroelectric materials were limited by device electronics and material technology at that time. Currently there is a huge research interest in utilizing ferroelectric thin films for electrically tunable microwave devices since they have large dielectric tunability, low loss, fast switching speeds and good power handling capability at GHz frequencies.

As modern portable electronic devices such as mobile phones and notebook computers have become more and more popular and these devices required nonvolatile memories. The ferroelectric random access memory (FeRAM) is one of the most anticipating candidates for satisfying this demand, because its power consumption is the lowest among the various semiconductor memories, and it also possesses nonvolatile and random access characteristics. There are other applications, such as ferroelectric capacitors non volatile random access

memories (NVRAMs), dynamic random access memories (DRAMs) and metal ferroelectric semiconductor field effect transistors (MFSFET).

The nonlinear dielectric behavior can also be used in devices such as tunable filters, varactor, variable phase shifters, tunable resonators, variable frequency oscillators, microelectronic mechanical systems, infrared sensors, actuators and transducers. Today's wireless communications and information systems are heavily based on microwave technology. The current trends indicate that in the future along with microwaves, the millimeter wave and terahertz technologies will be used to meet the growing bandwidth and overall performance requirements. The most of these devices need low voltage operation, therefore, a ferroelectric material with low coercive field or in thin film form is essential. It is not easy to fabricate these traditional ceramics in the form of thin film due to their fragile nature. In this regard, ceramic - polymer composite materials are emerging as a new class of electronic, microwave and dielectric materials.

In order to increase the flexibility on the market and functionality of RF/microwave transceivers, multi - band or multi - standard transceiver architecture solutions are pursued. In conventional implementation of multi - standard RF transceivers, multi - standard operation is usually achieved with independent RF front ends supporting each standard. But, it is undesirable due to the increased cost, size and weight with the increased number of target standards. Another approach is to make the RF transceivers electronically tunable so that it can be used to process the signal for more than one standard without introducing a separate hardware, and hence it is more economical and light weight. Since ferroelectric materials (e.g. BST, $BaTiO_3$, $CsNO_3$ etc.) have the property that their dielectric constant can be varied by changing the applied electric field across it; therefore, they can be used in the development of tunable RF front end circuits.

Ferroelectric materials are widely explored for tunable RF/microwave applications. The tunable RF devices developed using ferroelectric films have shown advantages in terms of high speed, higher power handling capabilities, lower cost and size in comparison with other possible solutions (e.g. MEMS). BST is widely used in tunable devices because of its large value dielectric constant and high tunability. The tunability of a particular material shows how much the dielectric constant of the material can be changed upon a certain applied electric field (bias). BST is a possible candidate for electrical tuneable microwave devices. BST is a potential candidate for tuneable microwave devices. $Ba_{1-x}Sr_xTiO_3$ is one kind of

composite material possessing perovskite type structure, which possesses the merits of both $BaTiO_3$ materials and $SrTiO_3$ such as a high dielectric permittivity, low dielectric loss, good stability and characteristics of semiconducting material, and good dielectric, ferroelectric properties and pyroelectric, nonlinear optical effect and so on.

Ferroelectric materials have sensitive physical properties, like dielectric constant, refractive index, magnetic permeability, polarization etc., to temperature, biasing electrical field, magnetic and mechanical stress. This cause effect relationship of the properties and external forces made them a very suitable choice for applications in microwave devices, optical devices, and electronics. Brief description of Ferroelectric materials paraelectric and ferroelectric phase properties is given below:

1. Stable spontaneous polarization in the polar phase (ferroelectric phase) that can be controlled by an external electric field.
2. Non polar phase (paraelectric phase) materials have randomly arranged dipole moments which cancels each other.
3. The dielectric parameters are very dependent on temperature and the properties are observed only within a definite range of temperature [5].

Barium strontium titanate ($Ba_{1-x}Sr_x\mathrm{Ti}O_3$) abbreviated as BST one of commonly used ferroelectric material is having above properties. Depending on the specific composition, temperature, BST can exhibit both paraelectric and ferroelectric behavior and is the most suitable ferroelectric material for RF/microwave devices fabrication. To fabricate microwave devices based on these materials, it is crucial to studs their electrical, ferroelectric and dielectric properties.

1.2 An overview of tunable microwave devices

In RF and microwave system components and circuits divided into active and passive. The microwave tunable passive devices primarily include phase shifters, filters, delay lines and network matching circuits in connection with such applications as antenna arrays, communications and radar transceivers. In the early days of microwaves devices, tuning was done mechanically or manually. Today, many circuit options are available to realize such electrical tunable devices whose performances are closely related to the choice of a technology. These options essentially include mechanical tuning, RF micro-electro-mechanical systems (MEMS) semiconductors, ferrites and ferroelectric materials. Electric

and magnetic fields (voltage, current), optical interactions or mechanical manipulations are used to achieve tunability in components based on them. The ranges and the speed of electrical tunability, control of power consumption, power handling capability, losses of microwave signal, potentials of integration, cost, and other parameters of the devices depend on the materials used, the controlling mechanisms (magnetic, optical, electrical, mechanical), and the design [6].

1.2.1 Review of non ferroelectric Technologies

Earlier all tunable circuits were mechanical, e.g. rotary vane adjustable waveguide phase shifter firstly proposed by Fox in 1947 [7]. Early mechanically tunable devices made use of coaxial lines or hollow metal waveguides and trimming screws/stepper motors/motors. Mechanical circuits are cheap, easy to fabricate and have very low loss and possess good power handling capability. However their main disadvantages are their size, low tuning speed, low cost, and sensitive to vibrations.

Semiconductor technology is one of very popular choice for making tunable integrated microwave devices. Semiconductors are promising in terms of integration possibilities, high tunability and much faster response speed. However, the linear decrease of the quality factor (Q) with frequency is the main disadvantage for high frequency >20GHz applications. Classically, the tuning can be made with continuous mode or switching using PIN diode or varactor diodes, respectively [8-9]. The tunable devices based on semiconductor are very small (in µms), very fast (<1µs for pin diode and <1 ns for FET), and have large electrical tunability, they can be easily integrated with other circuits for example in monolithic microwave integrated circuits (MMICs). In spite of these problems, semiconductors are widely used in tuning applications as they offer low cost, compact and integration advantages and allow faster tuning speeds. However, for large arrays antenna, such as phased arrays antenna with up to 10000 and more radiating elements, the power consumption and heat sink are the main problems forbade applications of semiconductor devices.

MEMS were started to use as tunable circuits, where tunability is obtained by the movement of a component which changes the capacitance of the device [10]. There are two types of MEMS circuits: switch and varactor [11]. MEMS varactors are small in size, low loss and most important, have very high Q factor value. However, the tuning speed and high

operating voltage are the main issues to be tackled [12-13] and they are sensitive to environmental conditions such as vibrations, moisture and temperature.

Ferrite has been used to fabricate microwave tunable devices [14-15], generally include phase shifters and filters. Ferrite phase shifters technology has been largely employed in military systems. However, they require strong magnetic fields, which will be power consuming. Besides, ferrite phase shifters are slow and cannot be used in application where rapid response is required.These microwave devices take advantage of a property of ferromagnetic materials to change its dielectric permeability with an applied DC magnetic field therefore allowing control of the phase constant of the waveguiding medium.

1.2.2 Ferroelectric Technology

Ferroelectric materials are of great interest due to the non-linear relationship between relative permittivity and applied bias electric field, which results in an ability to control relative permittivity by applying bias field. Due to the high relative dielectric permittivity, the sizes of tunable devices based on ferroelectrics are usually small. The breakdown strength of these ferroelectric materials is sufficiently high, so ferroelectric components have large tunability. Ferroelectric device have low power consumption and fast tuning speed of less than 1.0ns. These properties of ferroelectric materials make them promising candidates as tuning elements [16-21].

The main disadvantage in using ferroelectric materials for tunable wireless microwave devices is relatively high dielectric loss tangent (tanδ) of ferroelectric materials which leads to microwave dissipation. However late research indicated that the loss tangent can be reduced by improved thin film fabrication method and material enhancement such as by doping [22-28] or multilayering the ferroelectric thin film [29-31]. Although there are a lot of reports on the integration of ferroelectric materials with electrical tunable microwave devices, further advance and understanding of ferroelectric materials is required before more competitive devices can be developed. Also, research is required to develop prototypes of ferroelectric based varactors and miniature RF/microwave communication applications such as phase shifters and tunable matching networks etc.

1.3 Dielectric properties of ferroelectric thin films

In general, ferroelectric materials possess spontaneous electric polarization. The spontaneous electrical polarization of ferroelectric materials is due to electric dipoles. At a certain temperature range, the centers of the positive and negative charges in a crystal of such a material become displaced even without an external applied electric field. Groups of dipoles tend to align in the same direction instead of random arrangement, which will form a spontaneous polarization domain, to minimize energy. In experiment, spontaneous polarization of ferroelectrics implies a hysteresis loop in the response of polarization to an external bias electric field as shown in figure1.1.

The material relative permittivity ε_r is a complex quantity:

$$\varepsilon_r = \varepsilon_r^{'} - j\varepsilon_r^{''} \qquad (1.1)$$

By definition, the real part of the relative permittivity of ferroelectrics is proportional to the ratio of the electric polarization to applied electric field strength, which is corresponding to the slope of the P-E curve shown in figure1.1. This non-linear polarization for ferroelectric materials is the origin of the changing of relative permittivity $\varepsilon_r^{'}$ on an applied electric field, which is the key to their tunable devices applications. For description of the non-linear dependence of relative permittivity $\varepsilon_r^{'}$ on bias applied electric field and temperature, a phenomenological model could be expressed [32] as,

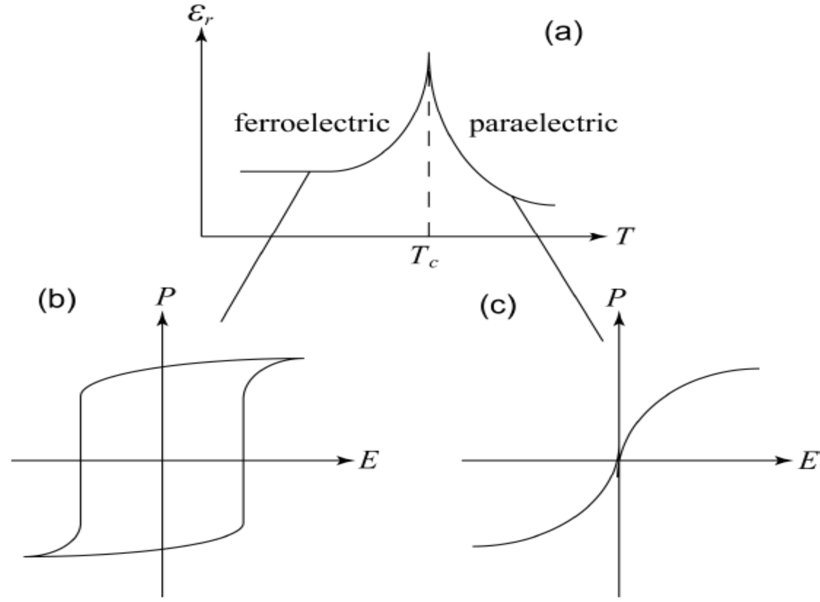

Fig. 1.1 Schematics of (a) relative dielectric constant as a function of temperature in different phases; hysteresis loop of polarization-electric filed in a (b) ferroelectric phase and (c) paraelectric phase.

$$\varepsilon_r^{'}(E,T) = \frac{\varepsilon_{00}^{'}}{\phi(E,T)} \qquad (1.2)$$

where $\phi(E,T)$ is phase shift which is function of applied field and temperature and $\varepsilon_{00}^{'}$ is a constant analogous to the Curie constant.

$$\phi(E,T) = \left[\left(\xi^2 + \eta^3\right)^{1/2} + \xi\right]^{2/3} + \left[\left(\xi^2 + \eta^3\right)^{1/2} - \xi\right]^{2/3} - \eta$$

$$\xi(E) = \left[\left(\frac{E}{E_N}\right)^2 + \xi_{st}^{\ 2}\right]^{1/2}$$

$$\eta(T) = \frac{\Theta}{T_c}\left[\left(\frac{1}{16} + \frac{T}{\Theta}\right)\right]^{1/2} - 1$$

where E_N =normalizing bias field, ξ_{st} = rate of crystal strain and Θ is Debye temperature. The change of relative permittivity $\varepsilon_r^{'}$ with frequency is small in the microwave frequency range, T_c is the Curie temperature, and $\varepsilon_{00}^{'}$ is a constant analogous to the Curie constant.

For microwave tunable device applications, the main focus of ferroelectric materials is to what extent the relative permittivity depends on applied electric field. This characteristic is represented by the tunability 'n' defined as the ratio of the relative permittivity of the material at zero electric field to its relative permittivity at non-zero bias electric field,

$$n = \frac{\varepsilon_r^{'}(E = o)}{\varepsilon_r^{'}(E)} \tag{1.3}$$

$$n_r = \frac{\varepsilon_r^{'}(E = 0) - \varepsilon_r^{'}(E)}{\varepsilon_r^{'}(E = 0)} = 1 - \frac{1}{n} \tag{1.4}$$

where n_r is the relative tunability. A schematic view of relative permittivity vs. bias electric field is show in fig.1.2 of ferroelectric materials in the paraelectric phase.

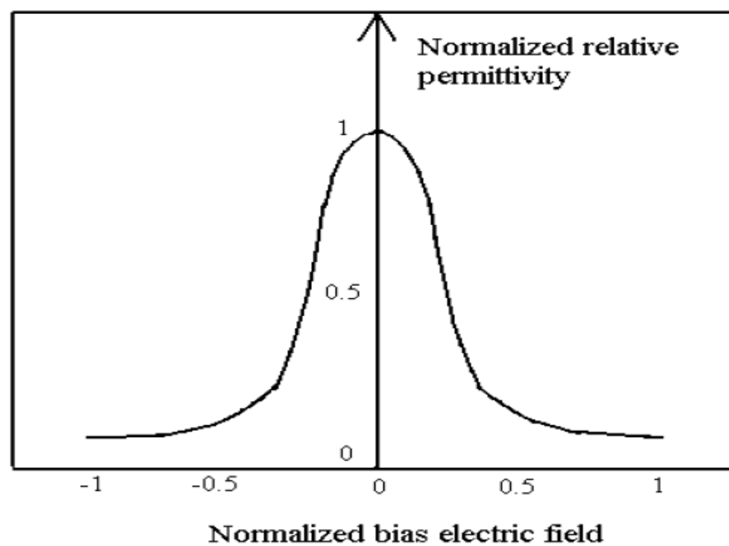

Fig.1.2. A typical relative permittivity vs. bias electric field characteristics of a ferroelectric material. The relative permittivity and bias electric field are normalized to their maximum values, respectively.

In the paraelectric regime above Curie temperature, the $\varepsilon_r^{'}$ shows non-linear dependence on the applied electric field. Also $\varepsilon_r^{'}$ decreases with temperature according to the Curie-Weiss relation,

$$\varepsilon_r^{'} = \frac{C}{(T - T_c)} \tag{1.5}$$

Another important property of ferroelectric materials is the loss tangent (tanδ), defined as the ratio of imaginary and real part of the relative permittivity,

$$\tan\delta = \frac{\varepsilon''_r}{\varepsilon'_r} = \frac{\mathrm{Im}(\varepsilon_r)}{\mathrm{Re}(\varepsilon_r)} \qquad (1.6)$$

1.3.1 Ferroelectric thin film varactors

Application of ferroelectrics to microwave devices began in 1960s. Ferroelectric thin films based varactor is one of very important applications in microwave components like resonator, phase shifter, filter and mixer. The desired electrical characteristics of varactor are high tunability and low loss tangent (tanδ) and also low leakage current at operating frequency and temperature [33, 34-35]. Various physical factors also affect the varactor properties like quality of ferroelectric thin film, varactor structure and quality of conducting metallization use to make electrode.

1.3.2 Basic structure of varactors

The structure of varactors plays major role to make a microwave component. There are two basic structure of varactor: planer plate structure and parallel plate structure as shown in fig.1.3 [36].

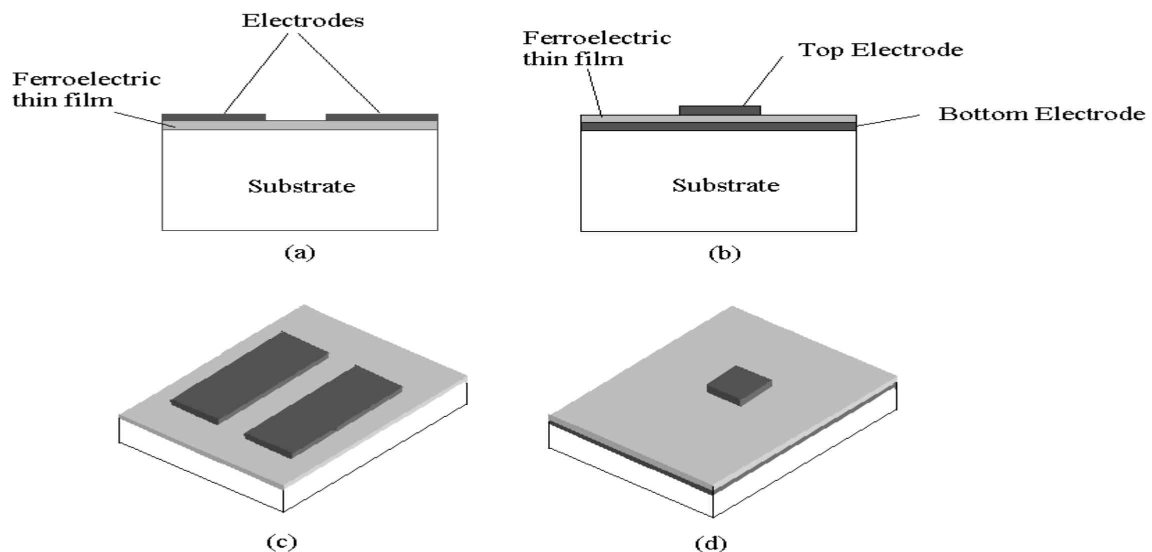

Fig.1.3 Layout of planar plate varactor (a) side view and (c) 3D view; parallel plate varactor (b) side view and (d) 3D view.

The planer varactor is shown in fig.1.3 (a) and (c) where a ferroelectric thin film is deposited on the suitable substrate (e.g. Si, MgO or sapphire) and electrode metallization is done on ferroelectric thin film. In case of parallel plate varactor as shown in fig. 1.3 (b) and (d), ferroelectric thin film is deposited on the bottom electrode followed by metallization is done on ferroelectric thin film.

When electric field is applied to varactor its relative permittivity changes from $\varepsilon'_r(E_1)$ to $\varepsilon'_r(E_2)$ and thus its capacitance changes from $C(\varepsilon'_r(E_1))$ to $C(\varepsilon'_r(E_1))$ with relative tunability,

$$n_r = \frac{C(\varepsilon_r'(E_1)) - (C(\varepsilon_r'(E_2)))}{C(\varepsilon_r'(E_1))} = 1 - \frac{C(\varepsilon_r'(E_2))}{C(\varepsilon_r'(E_1))} \qquad (1.7)$$

From eq. (1.7) for a given bias field on narrowing space between electrodes more electric field can be applied to the ferroelectric film and hence large value of tunability of ferroelectric thin film varactor can be achieved. For planer structure field is applied between electrodes across the gap where as in case of parallel plate varactor field is applied between top and bottom electrodes across the ferroelectric thin film. The ferroelectric thin films used in microwave tunable components generally have a thickness less than 1μm in parallel plate varactor is much thinner than the electrodes gap of the planar varactor (which is typically of the order of ten micrometer). As a result, the tuning voltage needed for planar varactor will be large; it is typically in the range of 100V. In case of parallel plate varactor, the bias voltage lies in the range of 1-20V, to give the same tunability.

However, the high relative permittivity and the small spacing between electrodes for parallel plate varactor will result in a large capacitance and limit its high frequency applications. Moreover, most of the parallel plate varactors are built with platinum bottom electrodes, which will contribute more loss of the device than in the case of the planar plate structure.

1.4 Barium strontium titanate ferroelectric thin films

Barium strontium titanate (BST) is one of very important ferroelectric material. It is mixer of$BaTiO_3$ (BTO) and $SrTiO_3$ (STO) and indicated as $Ba_xSr_{1-x}TiO_3$ (BST), is one of the widely investigated ferroelectric materials due to its high relative permittivity, moderate loss tangent and significant tunability. BST as a tunable device is preferred at room temperature

because its Curie temperature is below room temperature (~250K). Its Curie temperature depends on Ba/Sr ratio. The Curie temperature decreases linearly with increasing Sr concentration at a rate of 3.4°C per mole % Sr. Generally, a value of x in the range from 0.4-0.6 is desirable for room temperature application and thus thin film with Curie temperature around room temperature is used in this work as tuning elements of filter and phase shifter [37].

1.5 Outline of this dissertation

A brief outline of the organization of this dissertation is as follows:

CHAPTER – 2 describes fabrication and microwave characterization ferroelectric thin films. In which method of preparation of BST solution, chemical vapor deposition on Si (100), its structural analysis, electrical characterization and microwave characterization.

CHAPTER – 3 describescoupled microstrip line ferroelectric thin film varactor phase shifters. Here the results of the study of properties of coupled microstrip line, its RF excitation and phase shifter design are given.

CHAPTER – 4 describes measurement of whole results and discussion.

CHAPTER – 5 Conclusion and future scope of the work is presented.

CHAPTER – 2

FABRICATION AND MICROWAVE CHARACTERIZATION OF FERROELECTRIC THIN FILMS

2.1 Fabrication of ferroelectric thin films

Most of the device, fabrication requires advanced methods for synthesizing high-quality thin films to understand their properties and device performance. Current methods of fabricating ferroelectric thin films include: RF sputtering, Sol-gel method (chemical solution deposition) [38-39], molecular beam epitaxy (MBE), metal-organic chemical vapor deposition (MOCVD), and pulsed laser deposition (PLD). The first two provide polycrystalline or amorphous thin films, while the others can provide highly oriented thin films. Compared with other thin film deposition techniques, sol-gel method (spin coating) shows several advantages, some as rapid sampling of materials, homogeneity, stoichiometry control and simple preparation route. Today's sol-gel method becomes very popular technique to produce thin films having uniformity. In spite of above advantages this method also has some disadvantages: morphology and reproducibility. A comparison of different method is given in table 2.1.

2.1.1 Chemical solution deposition of BST undoped and doped thin film

The chemical solution deposition (CSD) methods have been widely used for perovskite thin films since the mid-1980s, mainly for ferroelectric thin films for electronic applications [40]. One of the major advantage of CSD method over other deposition techniques is an easier stoichiometry control as different film compositions (e.g. Ba/Sr ratio in the case of BST deposition) can be readily achieved by changing the composition of starting chemicals.

Normally, CSD deposition of BST thin film includes (1) precursor preparation, (2) film deposition and (3) pyrolysis (temperature range 200-400 ºC) and crystallization by high temperature annealing. The flow diagram is given in figure 2.1. For Mg doped BST magnesium acetate in proper amount is added just after 4th step and we get yellowish transparent solution.

Table 2.1 Advantages and Limitations of different techniques

Method	Advantages	Limitations
PLD	Rapid sampling of materials Quickly produce new materials Low temperature epitaxial growth	Morphology Point defect concentration Limited sample scale Uniformity High residual stress
RF Sputtering	Cost Uniformity Low temperature Scalability Standard IC processing	Point defect concentration Residual stress Stoichiometry control Slow deposition rate for oxide
MOCVD	Uniformity Morphology Composition control Low point defect concentration Scalability	Immature technology Precursor stability Precursor availability Expensive Down-time
MBE	Uniformity Composition control Precise atomic layering Extreme flexibility Scalability	Expensive Complexity Immature for oxide
CSD	Inexpensive, low capital investment Rapid sampling of materials Homogeneity Stoichiometry control Simple preparation route	Phase control Morphology Reproducibility

Figure 2.1 Flow chart for preparation of BST thin films

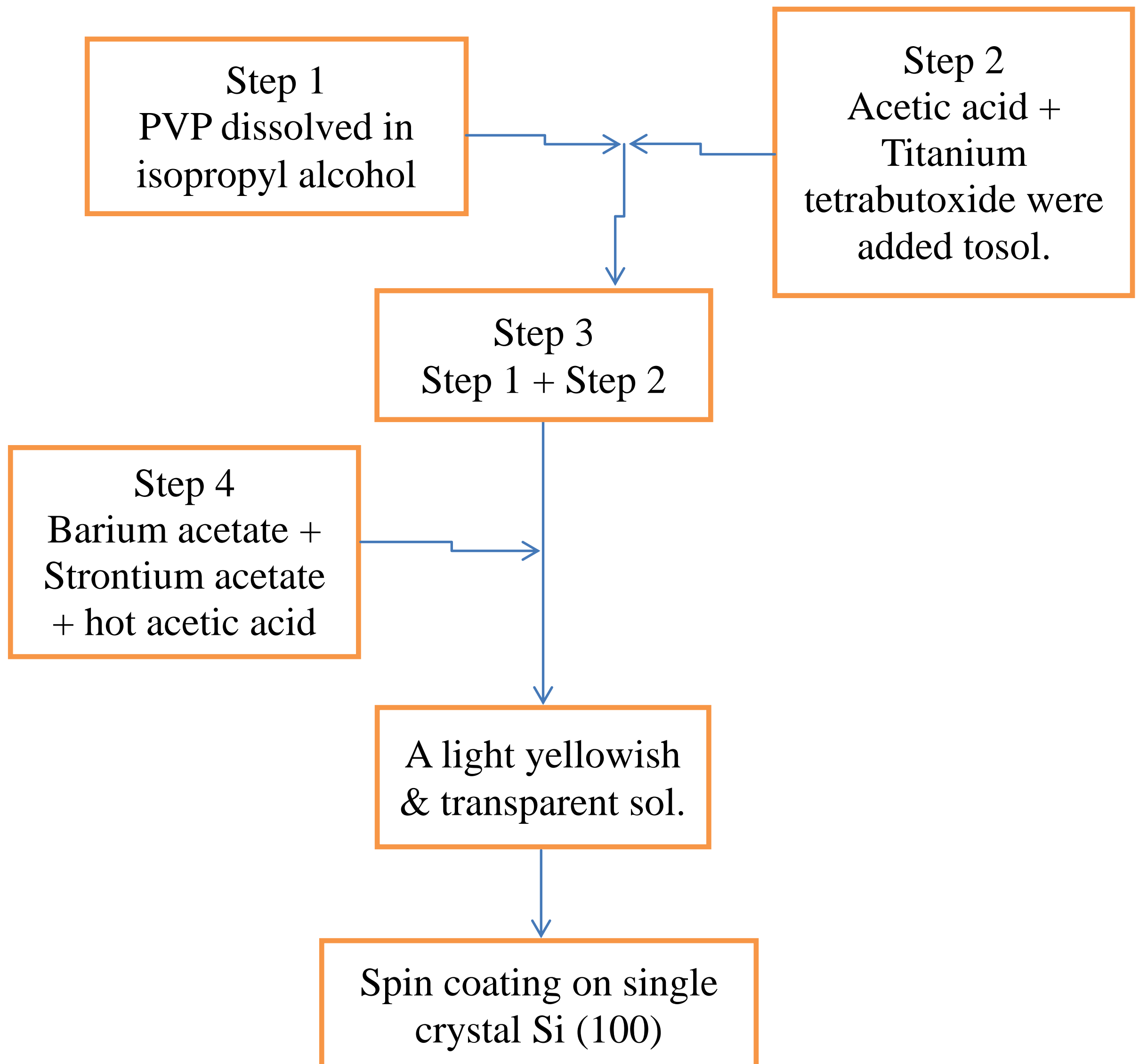

(a) Steps for undoped BST

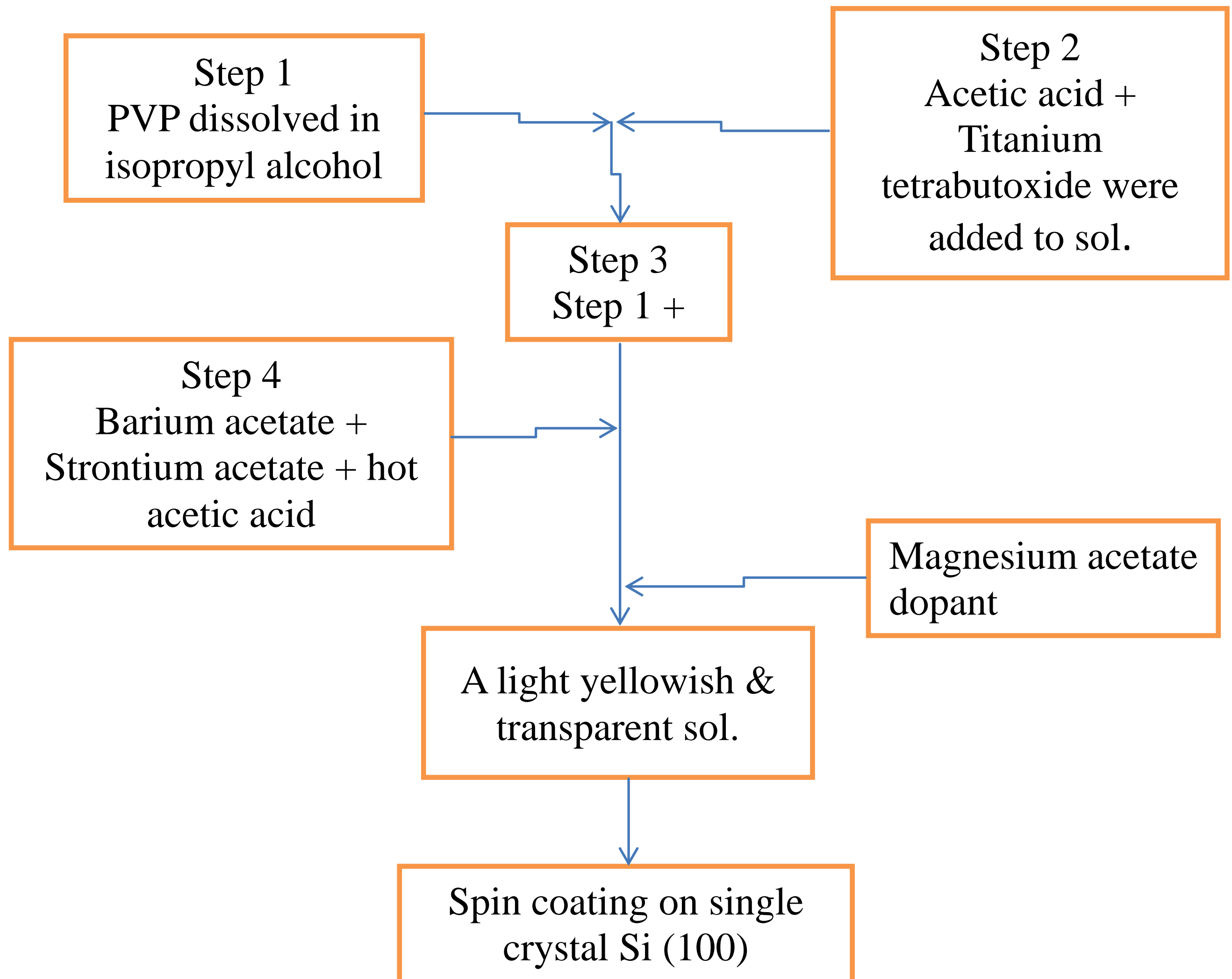

(b) Step for Mg doped BST

The molar composition of the BST sol. is Ti$(OC_4H_9)_9$/ Barium acetate/ strontium acetate/ PVP/acetic acid /isopropyl alcohol (to adjust viscosity of sol.) = 1:0.5:0.5:1:1:1. Finally we get BST solution which is light yellowish & transparent.

After getting BST solution it is spin coated on single crystal Si (100) substrate. It is done using spin coater whose speed is fixed at 2000 rpm for 45 second. After each spin coating of the sample is pyrolysis (normally 200-400 ºC) is done for 10 minutes. This process is done many times as per requirement of thickness of the deposited BST on the substrate. After getting desired thickness of BST on substrate it is sintered at 700 - 1200^{0}C for 2- 3 hours for proper crystallization of BST. If proper sintering is not done then BST become semi crystalline or amorphous which affects the properties of BST. The aluminum electrode was vacuum evaporated using a vacuum coating unit model – 12A4D. Electrode thickness is ~40 nm.

2.2 BST thin film characterization

BST film prepared by the above method was characterized using the following techniques.

1. For structural characterization: XRD was used, for Surface morphology FESEM and AFM were used.
2. For electrical characterization: C – V Characteristics were studied to obtained tunability.

2.2.1 Structural characterization

The X - ray diffraction measurements were performed to obtain the structural information in various types of pure and composite films using diffractometer. In Advanced Bruker D8diffractometer, the CuK_α radiations of wavelength 0.154 nm with nickel filter were used. The speed of goniometer was kept at 0.5°/min. The XRD scan of 50 wt. % composite films prepared by solvent cast method were also taken at different elevated temperature in the temperature range of 100 to 200°C. X -ray diffraction is a non-destructive and most powerful technique for determining the crystal structure, preferred orientation, crystallite size, lattice constants, stress and phase analysis, of thin films. The typical XRD pattern of BST thin film is given in figure 2.2.

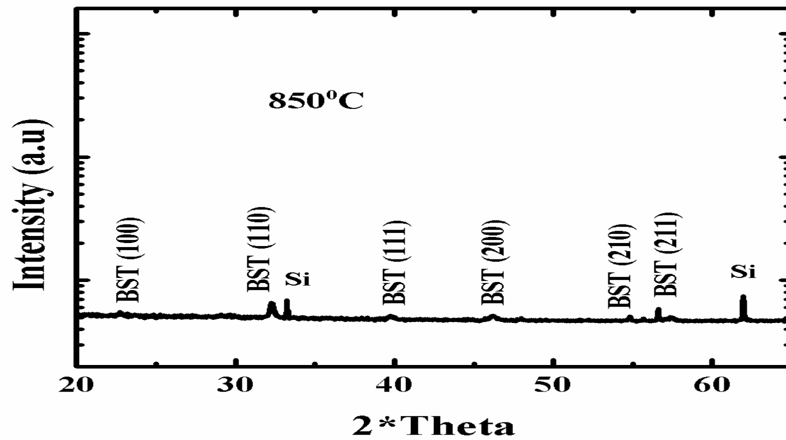

Figure 2.2 XRD pattern of 950nm BST thin film at 850^0C

It shows that BST thin film is polycrystalline in nature because of different peaks appears in the XRD pattern. The peaks at $2\Theta = 22^0$, 32^0 and 40^0 were analyzed and correspond to (100), (110) and (111) planes respectively. The BST thin film was also investigated using FEI XL30 scanning electron microscopy (SEM) to characterize the micro-structure during the film evolution. The SEM sample was coated by a thin gold layer to prevent charge accumulation during experiment. The SEM image is shown in Figure 2.3.

In Fig.2.4, the AFM image of the BST thin film is shown. The thickness of the film is measured by Tencor alpha step surface profiler after patterning the film in 2.5% HF solution and is found to be 945±5 nm. Therefore, approximately an 85 nm layer is obtained for each coating-crystallization cycle. The films were homogeneous and crack-free and the surface roughness is found from the AFM measurements to have a root mean square value of 12.75 nm and average grain size was 63nm.

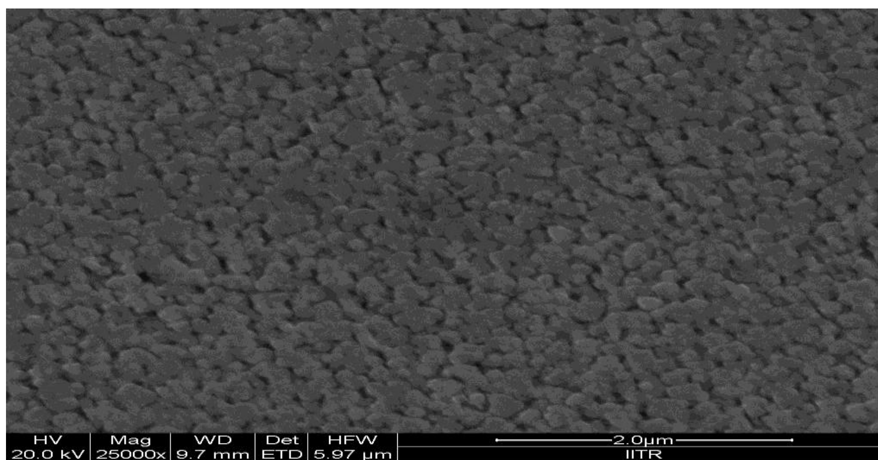

Figure 2.3. SEM images of ~950nm BST thin films by CSD method at 850^0C. The film is dense and without crack is clearly demonstrated.

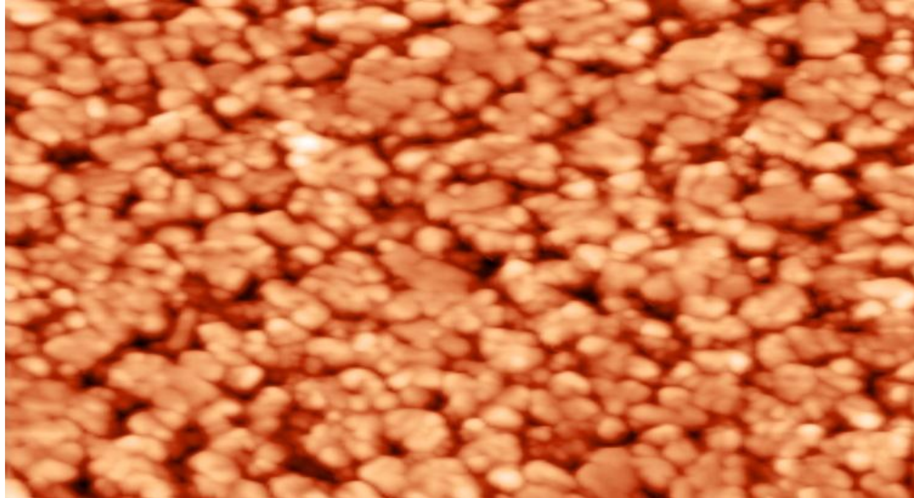

Figure 2.4 AFM images of ~950nm BST thin films by CSD method at 850^0C. The film is dense and without crack is clearly demonstrated.

2.2.2 Electrical characterization

To characterize the tunable properties of BST thin films, *i.e.* the capacitance as a function of applied voltage, planer plate capacitors were fabricated for the 950 nm BST thin films on a Si (100) wafer. After the BST deposition, a layer of 30nm thick Aluminum (Al) was deposited on top of it. The cross section view of planer plate varactor is given in (Fig.2.5).

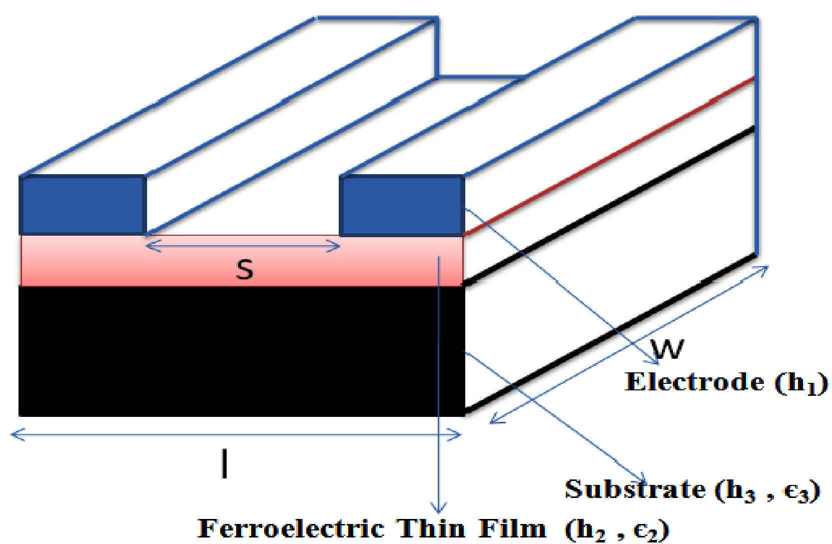

Fig.2.5. Cross section view of Si/BST/Al planer plate thin film varactor

The tunability of BST film is also calculated with the help of C-V plot using formula

$$\text{Tunability} = 100*(C_0 - C_V)/C_0 \qquad (2.1)$$

where C_0 is capacitance at zero bias and C_V is capacitance at applied bias voltage V

The Tunability of a specific material shows how much the dielectric permittivity of the material can be changed upon a certain applied bias electric field. The planer structure consists of three components, the ferroelectric film, substrate, and air. Its capacitance is formed by the capacitance of the stray fields in the ambient space (air) with dielectric permittivity $\varepsilon_1 = 1$, the capacitance of the ferroelectric thin film layer of thickness h_2 with dielectric constant ε_2, and the capacitance of the substrate of thickness h_3 with permittivity ε_3.

We represent the composite layered capacitor as three simple planar capacitors with uniform filler connected in parallel, and seek its capacitance as the sum of the three partial capacitances where C_1, C_2, and C_3, equal to gives the capacitances of the component parts of the planar capacitor, which are the fringing field in air, the ferroelectric film, and the substrate respectively [41]. From the Eq. (2.2) and (2.3), the permittivity of BST films was calculated.

$$C = C_1 + C_2 + C_3 \qquad \ldots\ldots\ldots\ldots\ldots\ldots\ldots\ldots\ldots\ldots\ldots\ldots\ldots \; (2.2)$$

$$C_1 = w\varepsilon_0 \frac{2}{\pi} \ln\left(\frac{4l}{s}\right)$$

$$C_2 = w\varepsilon_0 \frac{(\varepsilon_2 - \varepsilon_3)}{\left(\frac{s}{h} + (4/\pi)\ln 2\right)} \qquad \ldots\ldots\ldots\ldots\ldots\ldots\ldots\ldots\ldots\ldots\ldots\ldots \; (2.3)$$

$$C_3 = w\varepsilon_0 (\varepsilon_3 - 1) \frac{1}{\pi} \ln\left(16 \frac{h_3 - h_2}{\pi s}\right)$$

where ε_0 is permittivity of vacuum, ϵ_2 and ϵ_3 are permittivity of ferroelectric thin film and substrate respectively, h_2 and h_3 thickness of ferroelectric thin film and substrate respectively, l is length of thin film, W is width of thin film and s is space between electrode.

C –V measurement of the planer plate varactor is shown in fig. 2.6.The C - V measurements were performed at two fixed frequencies in different composite films using a Keithly 590 CV analyzer. The voltage was swept from -15 V to + 15 Vin 30 seconds in the forward cycle and +15 V to -15 V in reverse cycle with the same rate. The C - V characteristics of the composite films exhibit essential butterfly features of a ferroelectric material.

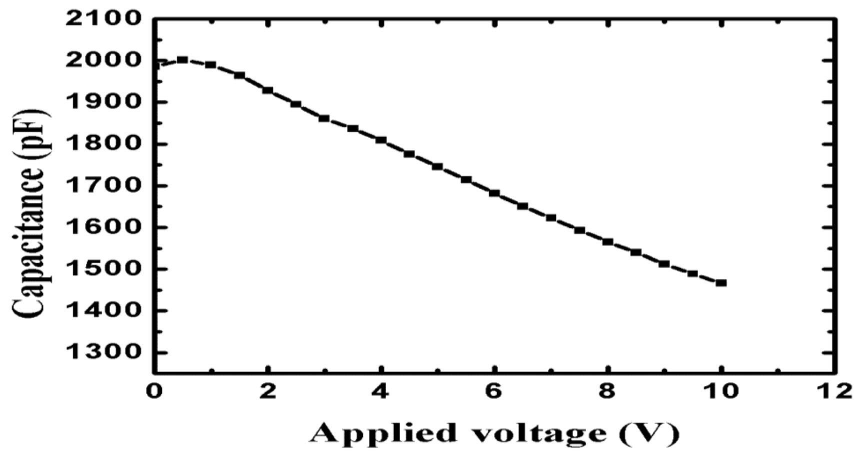

Fig. 2.6 C vs. V of BST thin film varactor

From the figure 2.6, it is clear that it shows tunability of ferroelectric thin film varactor i.e. as bias voltage changes its capacitance also changes and we get maximum capacitance at zero volts. Fig.2.7 shows the loss tangent of ferroelectric thin film, as the bias voltage increases the loss tangent decreases and maximum loss occurs at zero volts. The loss tangent measurements of BST thin film were done using "590 C-V analyzer". At microwave frequencies, usually the conductor loss due to the interconnecting lines and electrodes is a main contributor to the overall loss of ferroelectric thin film BST capacitors. The formula to calculate loss tangent is given below.

$$\text{Loss tangent} = \frac{G}{Cws} \tag{2.4}$$

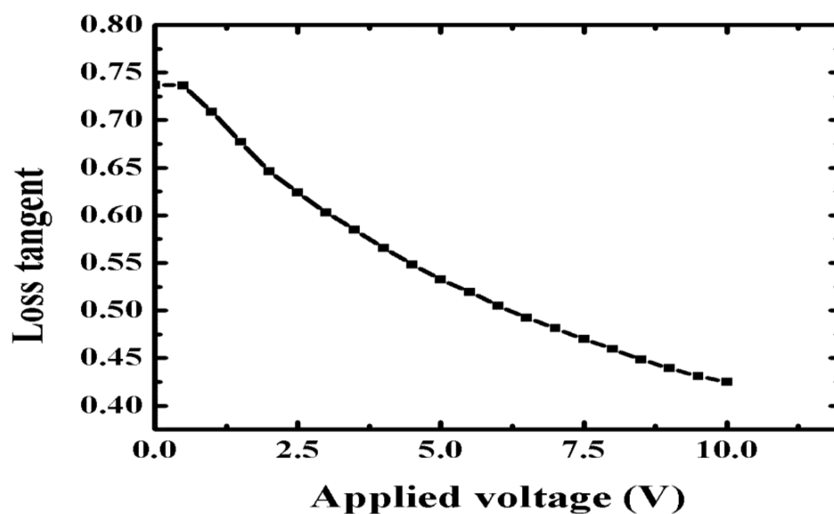

Fig. 2.7 Loss tangent vs. V of BST thin film varactor

2.3 Microwave measurement techniques for ferroelectric thin films

It is very important to characterize the high frequency dielectric permittivity and tunability of ferroelectric materials for microwave applications. For low frequencies (< 100 MHz), the varactor which is made of any form of ferroelectric material is considered as a lumped element since its dimensions are much less than the wavelength of the electromagnetic signal. The capacitance and loss tangent of the varactor can be measured directly by a standard impedance analyzer. At higher frequencies (RF/microwave), direct measurements of the capacitances are less applicable because, at higher frequencies, the dimensions of the varactors become comparable with the wavelength of the electromagnetic wave used and they cannot be considered any more as lumped elements. Generally speaking, the microwave measurement techniques for characterizing dielectric composites, ceramics and bulk ferroelectric crystals admit non resonant methods and resonant methods [42]. Ferroelectric thin films are normally characterized using planar-circuit methods, and almost all the dielectric properties, including the dielectric relaxations and electric tunability, are needed to be studied. There are three measurement methods, including lumped capacitance measurement method, coplanar waveguide transmission line method, and coplanar resonator method. In this section we will discuss only lumped capacitance measurement method.

2.3.1 Lumped capacitance measurement method

The dielectric permittivity of thin film is calculated from the capacitance and the loss factor of the ferroelectric thin film, is estimated from the quality factor of the capacitor. The two important prospect of this method are the capacitor design and the capacitance measurement.

Although ferroelectric thin film varactor capacitors have been created in many different designs, they basically consist of two structural types: the parallel plate type (trilayer capacitor) and the planar type (e.g. interdigital capacitor). Figure 2.8 shows the configurations of the two types of ferroelectric thin film varactor capacitor. Characterization of ferroelectric thin film capacitors at RF/microwave frequencies is complex by several factors. At these frequencies, series inductance related with the electrode geometry introduces a self-resonant frequency that limits the useful measurement and operating bandwidth. The high capacitance density of the thin films also means that capacitors supposed for use in this frequency range will have rather small electrode areas. Measurement interpretation is also more complex, as new loss mechanisms become important in the GHz range that may not be

obvious at lower frequencies (dielectric relaxation processes, interfacial losses originating from electron transfer between the electrodes and surface states, and skin-effect losses in the electrodes) [43]. Here are some methods reported on-wafer characterizations which are based on parallel plate capacitor and interdigital capacitor (IDC), structure as shown in fig. 2.8.

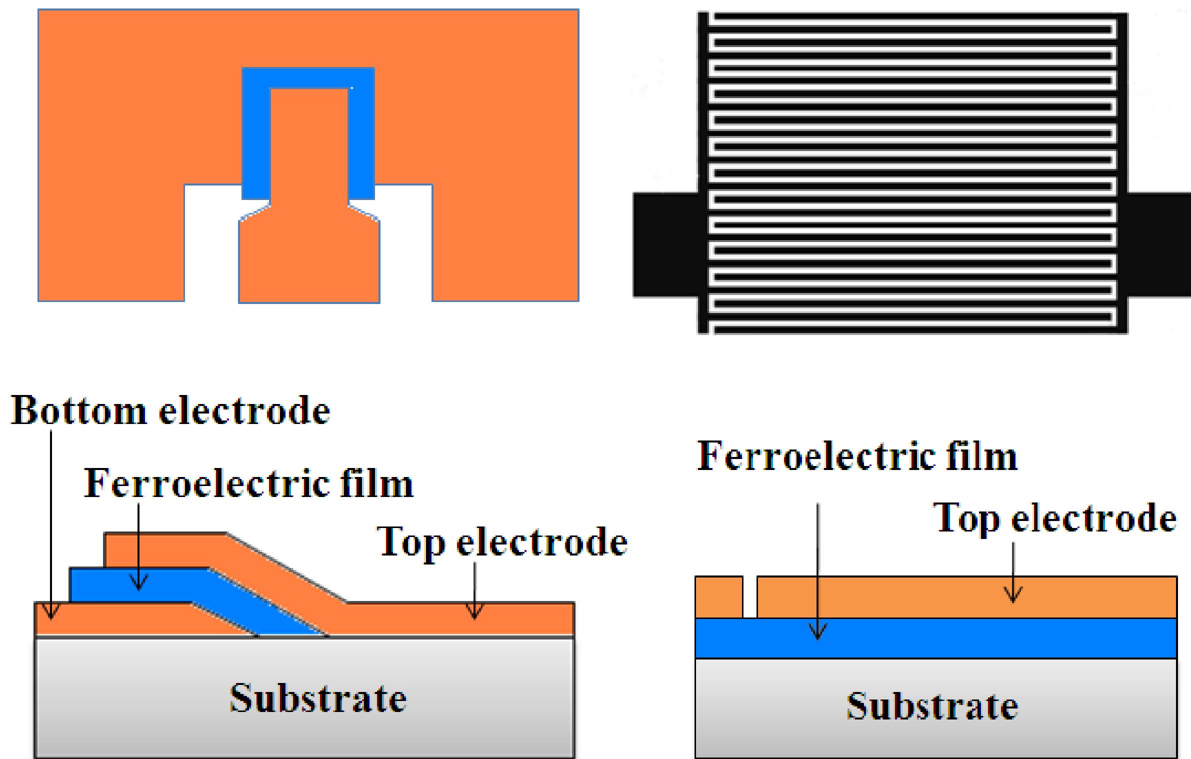

Figure 2.8 the plane-view and cross sections of ferroelectric thin films capacitors.(a) Parallel plate capacitor; (b) interdigital capacitor.

A simple and generally used test structure for one-port network analyzer measurement using ground-source-ground (GSG) probes has been proposed [44,45]. As shown in Figure 2.8 (a), the equivalent circuit of the capacitor can be represented by lumped elements of intrinsic capacitor admittance, parallel and series stray admittances. The intrinsic capacitor admittance Y can be expressed in terms of S_{11}as:

$$Y = G + j\omega C = \frac{1}{Z_0}\left(\frac{1 - S_{11}}{1 + S_{11}}\right) \qquad (1)$$

where C and G are the capacitance and conductance of the capacitor, ω is the measured angular frequency, $S_{11}$is the measured complex reflection coefficient from a vector network analyzer (VNA), and $Z_0$is the characteristic impedance (50Ω) of the transmission cable. The relative dielectric constant (ε_r) and dielectric loss tangent (*tan δ*) of ferroelectric thin film can be derived from equation (1):

$$\varepsilon_r = C \cdot h / A \cdot \varepsilon_0 \quad (2)$$

$$tan\delta = G / \omega \cdot C \quad (3)$$

A key issue found in evaluating the high-frequency dielectric properties of parallel plate capacitors is the exact evaluation of parasitic. In particular, the series resistance that prevails high-frequency loss should be completely excluded to exact estimate the dielectric loss.

In the interdigital capacitor (IDC) shown in Figure 2.8 (b), the substrate of the capacitor belongs to two layers: ferroelectric thin film (in this case BST) with dielectric constant ε_2 and the substrate (Si (100)) with dielectric constant ε_1. Conformal-mapping-based models for IDC on layered substrates have been applied to the device data [46]. By definition, these models are only relevant at frequencies which are sufficiently low that the device is electrically small. The relative dielectric permittivity of the thin film can be calculated given the geometry of the IDC, the thickness of the ferroelectric thin film, the thickness and dielectric permittivity of the substrate, and the measured capacitance. The IDC is modeled by a parallel resistor-capacitor model [47] for which the admittance reads

$$Y = Y_0 \frac{1 - S_{11}}{1 + S_{11}} = jwC \quad (4)$$

where Y_0 is the reference admittance and $S_{11}$is the reflection coefficient of the calibrated device. C is defined here as complex capacitance, where Re[C]is the usual capacitance and Im[C] =−G/ω, where G is the conductance. Each partial capacitance is showed as the product of a known factor, depending only on the IDC geometry, and a partial dielectric permittivity of the form

$$\varepsilon_{eff,x} = 1 + \frac{1}{2} q_{1,x} (\varepsilon_1 - 1) + \frac{1}{2} q_{2,x} (\varepsilon_2 - \varepsilon_1) \quad (5)$$

In this linear expression, the index x stands for 2, $q_{1,\ x}$ and $q_{2,\ x}$ are filling factors depending only on the IDC geometry. Filling factor is a measure of the percentage of the bias electric fields in a transmission line that cut through the substrate. In non-TEM transmission lines such as CPW and microstrip, the electric fields cut through two (or sometimes more) dielectric materials. For a given capacitor, its capacitance can be calculated according to the equations (5).

CHAPTER – 3

COUPLED MICROSTRIP LINE FERROELECTRIC THIN FILM VARACTOR PHASE SHIFTERS

In this work phase shifter uses coupled microstrip line as dc electrodes to polarize a ferroelectric thin film. The coupled microstrip lines are frequently used in microwave integrated circuits, where couplers or filters have been realized within the circuitry. This chapter describes the coupled microstrip line phase shifter (CMPS) using BST thin film varactors with planer plate electrode.

3.1 Properties of coupled microstrip line

Some basic design equations for coupled microstrip lines useful for design of phase shifters are briefly described in this section.

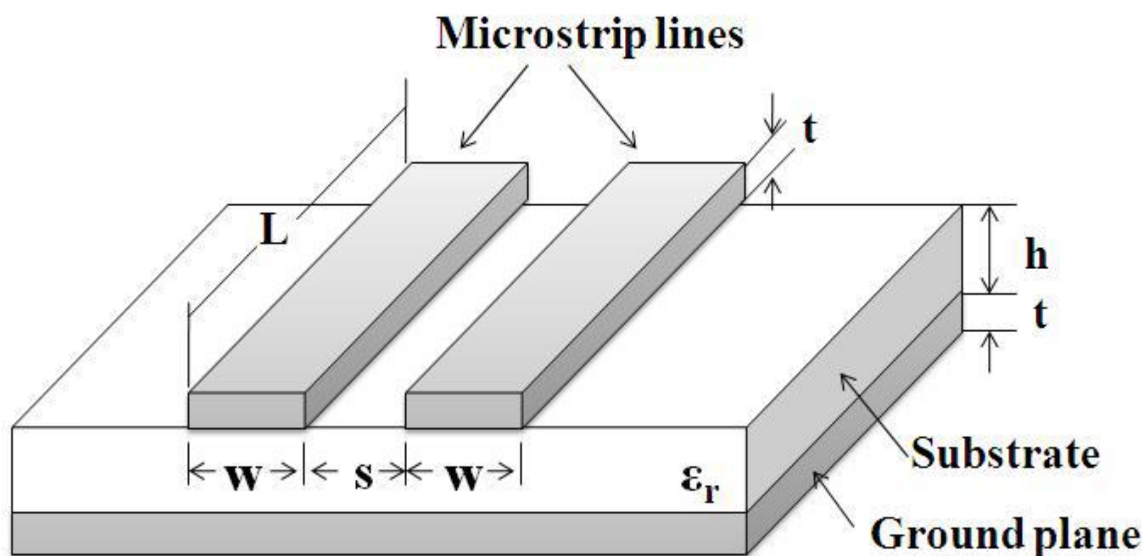

Figure 3.1 a conventional coupled microstrip lines

This structure has two microstrip lines of width w at a distance of s. The two lines can carry two cardinal quasi-TEM modes, the even mode and the odd mode, which have different effective dielectric permittivity (i.e., different phase velocities of their waves) and different dispersion properties because of the different field structures of the modes. The electric (E)

and magnetic (H) fields associated with each mode are indicated in Figure 3.2. For an even-mode excitation, both microstrip lines have the same voltage potentials or carry the same sign charges (say'+'), consequent in a magnetic wall at symmetry plane, as shown in Figure 3.2 (a). For the odd-mode, both microstrip lines have the opposite voltage potentials or carry the opposite sign charges, so that the symmetric plane is an electric wall, as indicated in Figure 3.2 (b). In general, these two modes will be excited at the same time. However, they propagate with different phase velocities because they are not pure TEM modes, which mean that they experience different dielectric permittivity. Therefore, the coupled microstrip lines are characterized by the characteristic impedances and the effective dielectric permittivity of the even- and odd- modes [48].

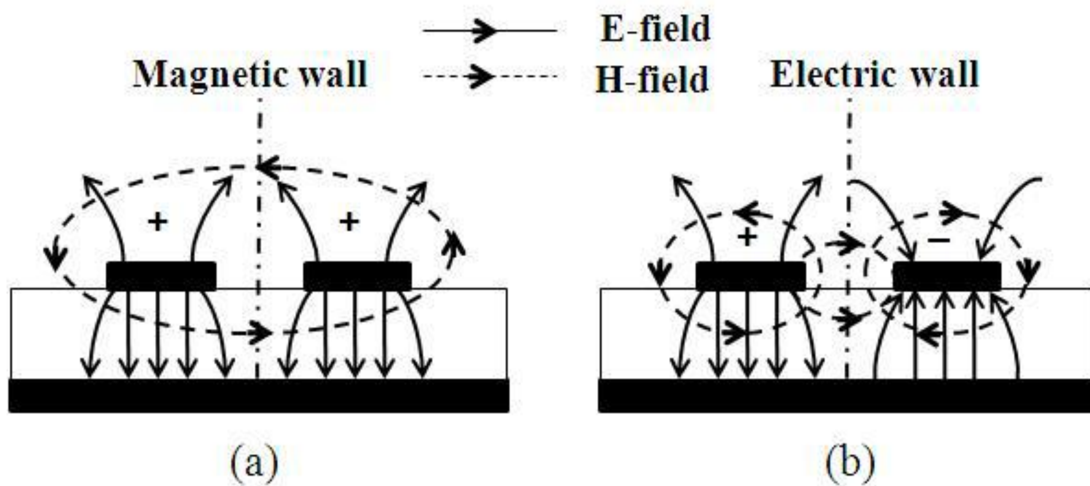

Figure 3.2 Field distributions resulting from (a) even-mode and (b) odd-mode excitation of the coupled microstrip lines.

The most simple and widely used expressions for symmetric coupled microstrip line synthesis are provided by Garg and Bahl [49]. The even- and odd- mode characteristic impedances Z_{even} and Z_{odd} can be obtained from the capacitances.

$$Z_{even} = \frac{1}{C\sqrt{C_{even}^{air}.C_{even}}} \tag{3.1}$$

$$Z_{odd} = \frac{1}{C\sqrt{C_{odd}^{air}.C_{odd}}} \tag{3.2}$$

where C_{even} and C_{odd} are even and odd mode capacitances, C_{even}^{air} and C_{odd}^{air} are even and odd mode capacitances of coupled line where air as a dielectric medium.

Effective dielectric permittivity ε_{even} and ε_{odd} for even and odd modes, respectively, can be obtained from equations (3.1) and (3.2).

$$\varepsilon_{evebn} = \frac{C_{evev}}{C_{even}^{air}} \tag{3.3}$$

$$\varepsilon_{odd} = \frac{C_{odd}}{C_{odd}^{air}} \tag{3.4}$$

3.2 Phase shifter design

3.2.1 Calculation of phase shift and tenability

The coupled microstrip line phase shifter is fundamentally a high impedance transmission line periodically loaded with ferroelectric thin film varactors. The equivalent lumped element circuit of the phase shifter is similar with that of the coplanar waveguide phase shifter. In the figure 3.3, ΔL is distance between varactors or length of unit cell, L_0 and C_0 are lumped inductance and capacitance of unit cell. The Substrate is Si (100) which has thickness of 500μm and dielectric constant is 510. A schematic structure and equivalent circuit of the coupled microstrip (CM) lines phase shifter is shown in figure 3.3.

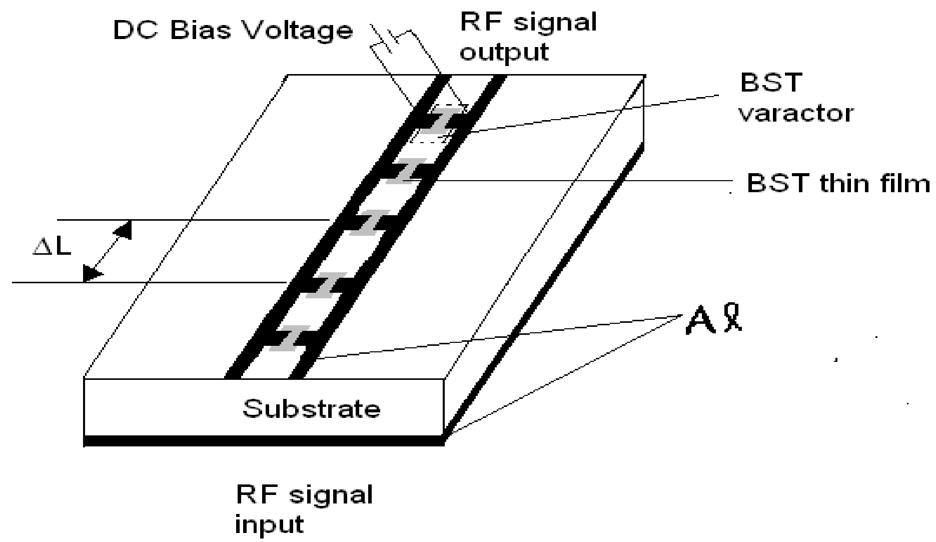

(a)

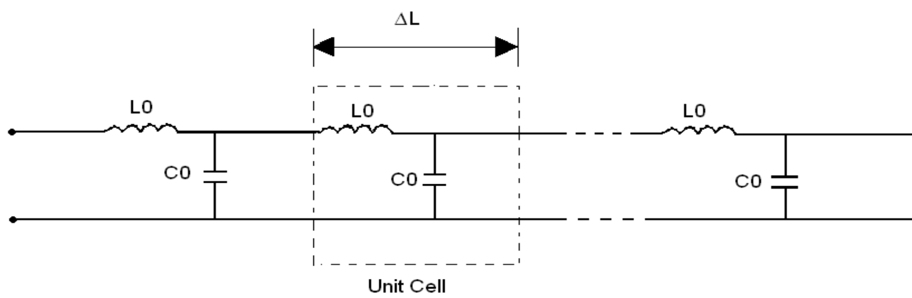

(b)

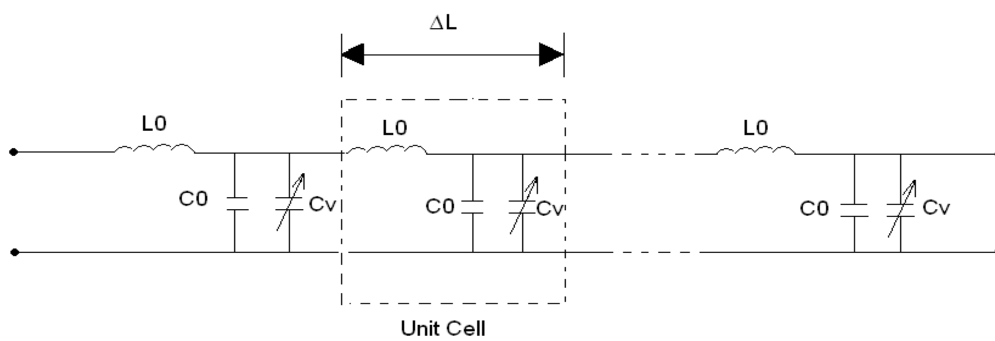

(c)

Figure3.3 Schematic structure of a CM phase shifter periodically loaded with thin film varactors and its circuit approximation (a) schematic layout (b) equivalent circuit of coupled lines before loaded with varactors (c) after loaded with BST thin film varactors

The characteristic impedance and propagation constant of the unloaded coupled microstrip lines shown in figure 3.3(b) are presented below:

$$Z_0 = \sqrt{\frac{L_0}{C_0}} \tag{3.5}$$

$$\beta_0 = \omega\sqrt{L_0 C_0} \tag{3.6}$$

Varactors with capacitance C_{v1}at zero bias state are loaded periodically between the coupled microstrip lines, as seen in the equivalent circuit of figure 3.3(c), the capacitance per unit length is increased and the inductance per unit length for these coupled lines remains unchanged. The characteristic impedance, propagation constant and phase shift are,

$$Z_0 = \sqrt{\frac{L_0}{C_0 + C_{v1}/\Delta l}} \tag{3.7}$$

$$\beta_0 = \omega\sqrt{L_0(C_0 + C_{v1}/\Delta l)} \tag{3.8}$$

$$\phi_1 = \omega l\sqrt{L_0(C_0 + C_{v1}/\Delta l)} \tag{3.9}$$

After a bias voltage of V is applied to the varactors capacitor, the corresponding characteristic impedance, propagation constant and phase shift are,

$$Z_0 = \sqrt{\frac{L_0}{C_0 + C_{v2}/\Delta l}} \tag{3.10}$$

$$\beta_0 = \omega\sqrt{L_0(C_0 + C_{v2}/\Delta l)} \tag{3.11}$$

$$\phi_2 = \omega l\sqrt{L_0(C_0 + C_{v2}/\Delta l)} \tag{3.12}$$

where C_{v2} is the capacitance of the varactors at bias state. From equation (3.9) and (3.12), it can be seen that since the capacitance of the loading varactors is electric field dependent, the properties of the loaded microstrip lines, such as the characteristic impedance, phase velocity,

propagation constant, are functions of electric field. Therefore, the phase shift for a given length of transmission lines by,

$$\Delta\phi = \phi_2 - \phi_1 = \omega l\sqrt{L_0(C_0 + C_{v2}/\Delta l)}\ \omega l\sqrt{L_0(C_0 + C_{v1}/\Delta l)} \qquad (3.13)$$

Therefore, tunability of the phase shifter between the two states can be calculated,

$$\frac{\Delta\phi}{\Delta V} = \frac{2\pi f\sqrt{L_0\left(C_{v1}/\Delta l\right)}}{2\sqrt{(C_0 + C_{v1}/\Delta l)}}\frac{\Delta\left(C_{v2}/C_{v1}\right)}{\Delta V} = \frac{\beta_0}{2}\left(\frac{Z_0}{Z_1} - \frac{Z_1}{Z_0}\right).\Delta\frac{\left(C_{v2}/C_{v1}\right)}{\Delta V} \qquad (3.14)$$

3.3 Fabrication of phase shifter

At the first step BST thin film is deposited on Si (100) substrate using spin coating according to the pattern on substrate. After deposition of desired thickness of the BST thin film it is pyrolysed (300^0C to 400^0C) and then sintered (750^0C to 1200^0C). After this step for electrode Al metallization (~50nm) is done on it and at the bottom of substrate. Flow chart of fabrication process of BST thin film varactor phase shifter is given below.

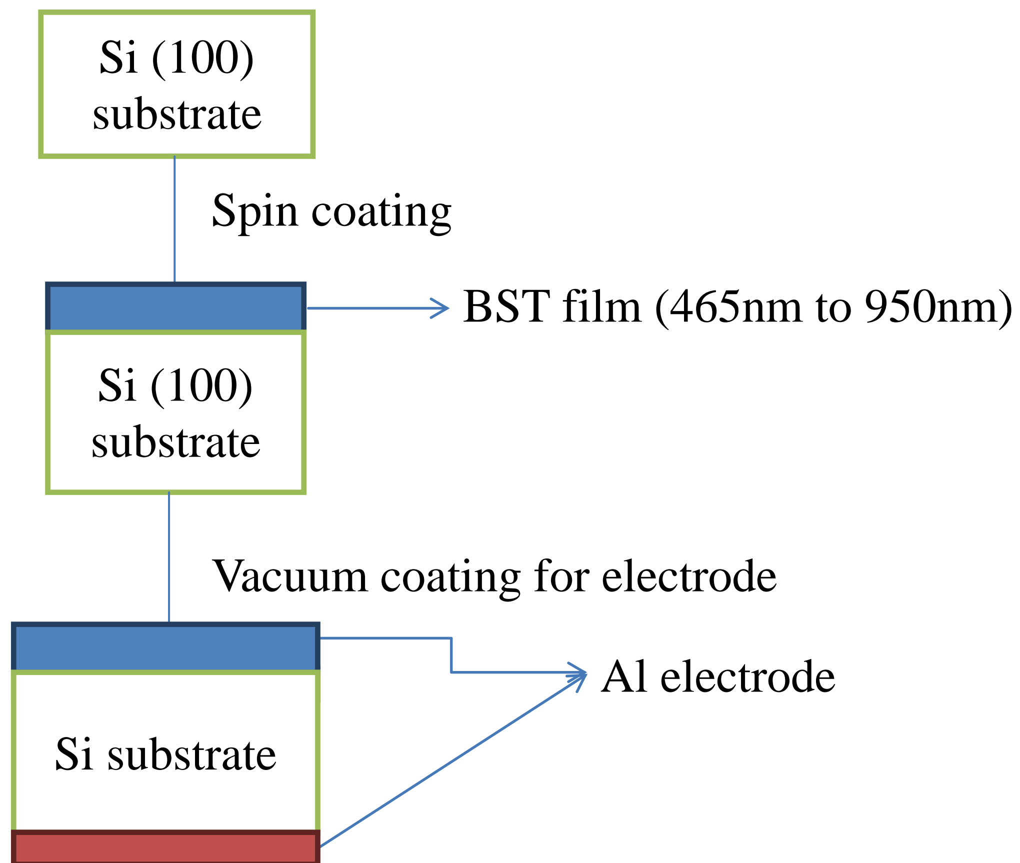

Figure3.4 Fabrication process flow chart for thin film deposition and metallization of BST varactor.

CHAPTER 4

MEASUREMENT RESULTS AND DISCUSSION

4.1 Experimental results of XRD:

XRD pattern of BST thin film is given below.

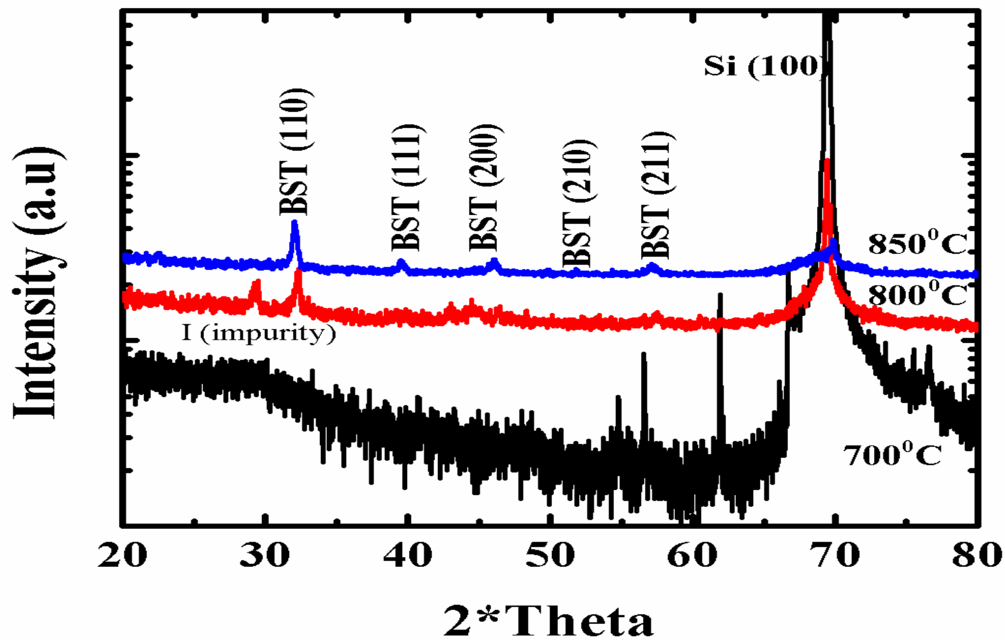

Figure 4.1.1 XRD pattern of undoped BST film at different temperatures

Figure 4.4.1 we shows that as the annealing temperature was increased the x-ray peak intensity increased and the full-width-half-maximum (FWHM) decreased indicating increased crystallinity and an increase in grain size with increasing sintering temperature up to 850^0C. The film annealed at 850^0C has better crystallization, uniformity and larger grain size than films annealed at 700^0C and 800^0C.The BST film annealed at 800^0C gives some impurity content at ~29^0. Similarly from figure 4.1.2 we can see that BST films having thickness 950nm has better crystallization than 715nm, 530nm and 465nm thick films. So overall, we can say that the films annealed at higher temperature and are thick have better grain size, less porous, better crystallization and hence higher dielectric constant.

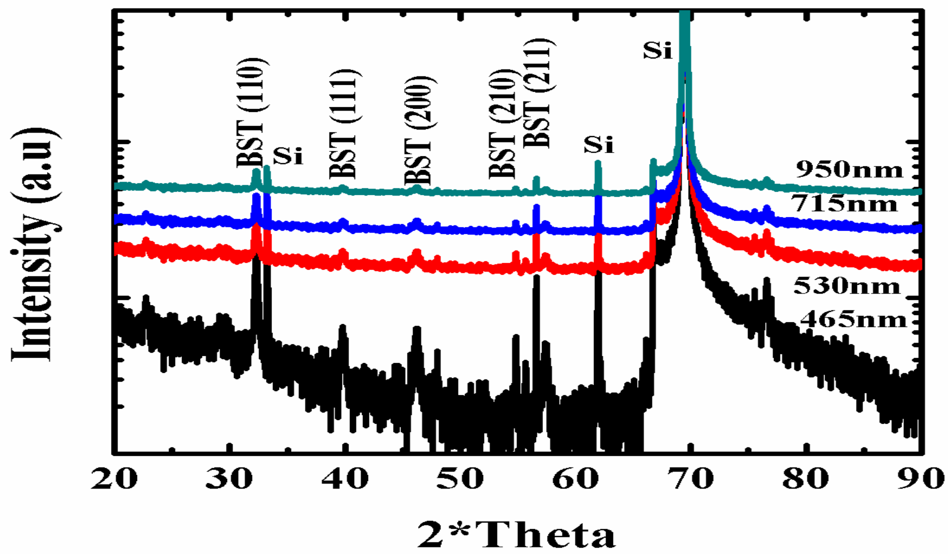

Figure 4.1.2XRD pattern of undoped BST film at different film thickness

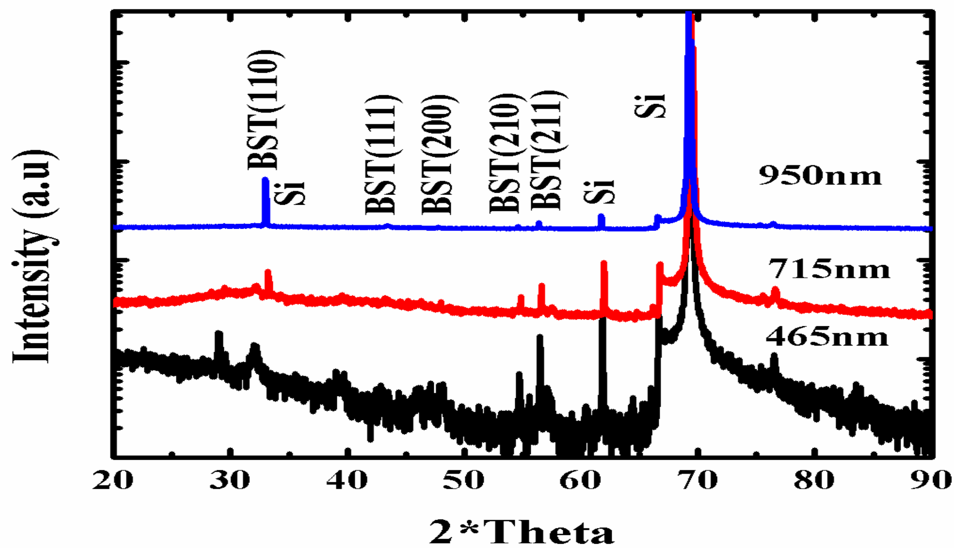

Figure 4.1.3 XRD pattern of 5 mol% Mg doped BST film at different film thickness

The direct comparison of the XRD data for the undoped and doped films showed that the peak intensity is larger for undoped film and FWHM of the Mg doped thin film was larger than that of the undoped BST thin films at all film thickness which indicate a smaller grain size for the Mg doped BST thin films with respect to that of the undoped films, hence smaller dielectric constant in case of Mg doped case.

4.2 Experimental results of FESEM:

Surface morphology and cross section of a sample at different temperature and sample having variable thickness at fixed temperature is given below.

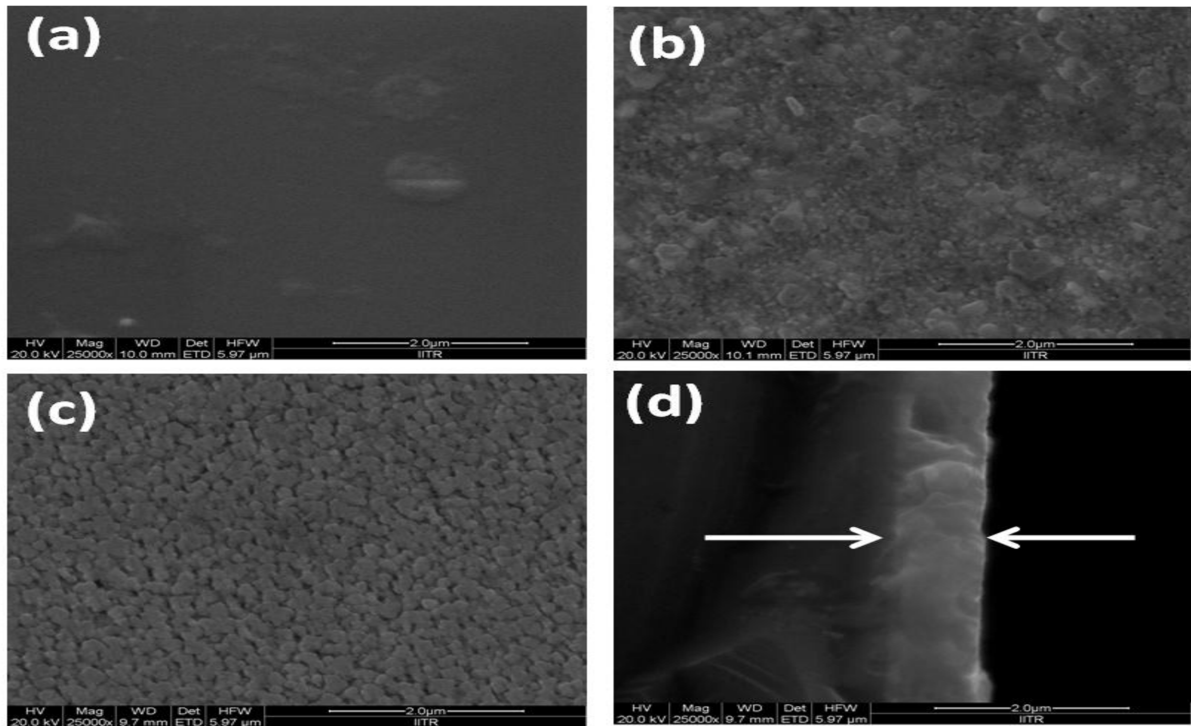

Figure 4.2.1 Surface morphology of 950nm BST film (a) at 700^0C (b) at 800^0C (c) at 850^0C and (d) cross section

From the above figure 4.2.1 we observe that grain size is more clear and uniform in (c) i.e. at 850^0C as compared to (b) and (a). The FESEM analyses supports the x-ray results in that the 700◦C sintered thin films were amorphous and that the microstructure became fully developed after annealing at 800^0C. The 850^0C annealed undoped and Mg doped films possessed a dense well crystallized microstructure with a homogeneous cross-sectional thickness of 950 nm. The films were polycrystalline and were composed of granular multigrains randomly distributed throughout the film thickness. The FESEM micro graphs how a clear structural delineation between the film and the Si substrate. No amorphous layer or voiding/defects was observed at the film-Si interface. This defect free and structurally abrupt interface bodes well for the excellent mechanical integrity and good adhesion characteristics of the undoped and Mg doped BST film-Si substrate.

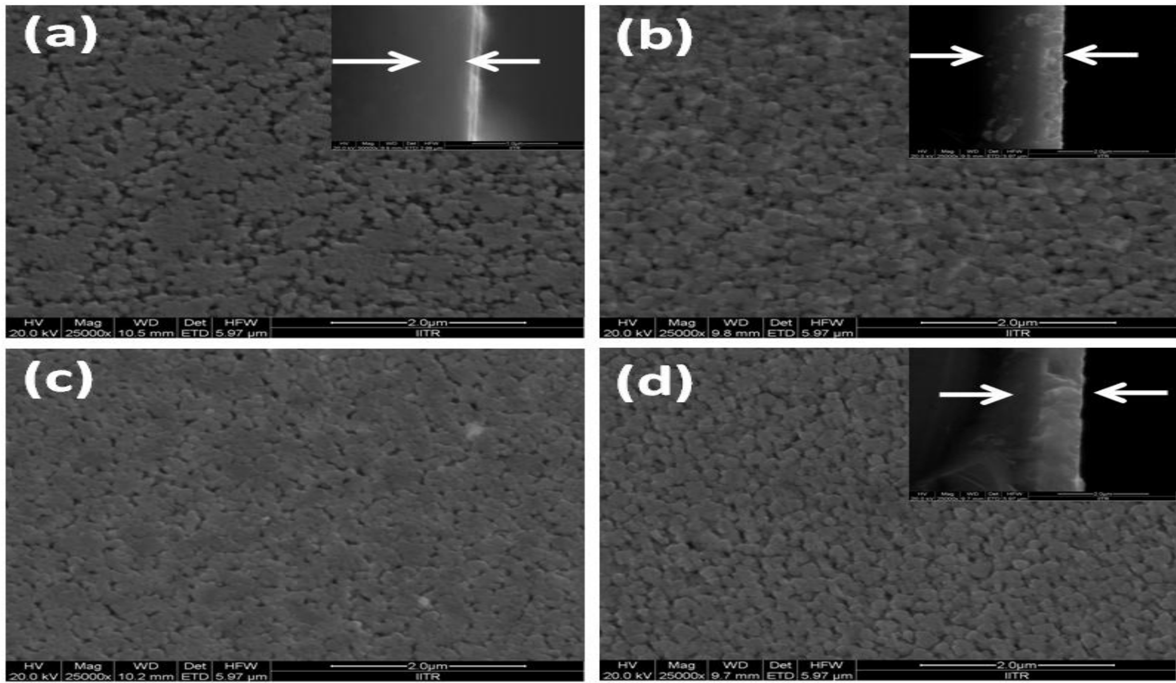

Figure 4.2.2 Cross section at 850^0C (a) 465nm (b) 530nm (c) 715nm (d) 950nm

In figure 4.2.2 we observe that larger grain size, uniformity and less porous, hence better crystallization in (d) as compare to (c), (b), (a). Similarly (c) is better than (b) and (a). So we conclude that on increasing thickness we can get better thin film having better crystallization and uniformity. The FESEM analyses support the x-ray results. Over all we conclude that films having annealed at higher temperature and are thick results in a better BST film.

4.3 Experimental results of AFM:

The AFM images of undoped and doped BST thin film are shown in figure 4.3. In figure 4.3 (a) and (b) are 2D images of undoped and doped BST respectively, (a) is more uniform and crack free as compare to (b) whereas (c) and (d) are the 3D image of undoped and doped respectively , it also supports figures (a) and (b).

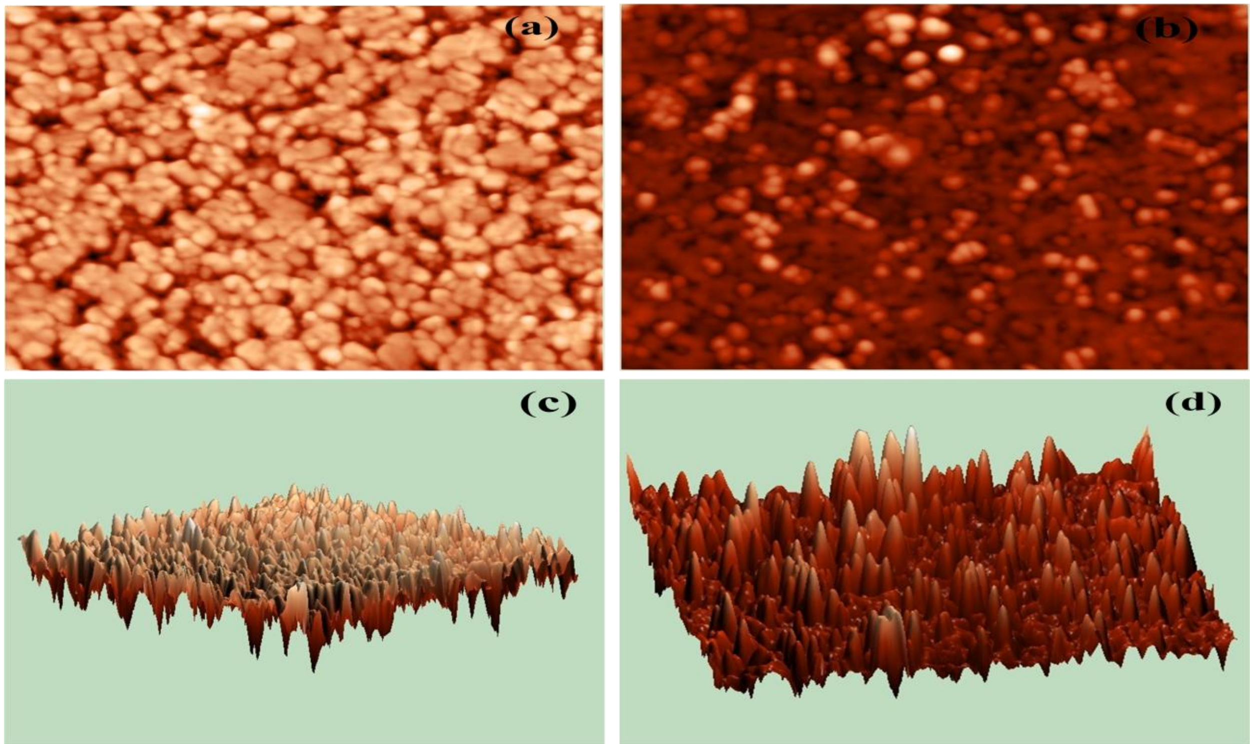

Figure 4.3AFM image of 715nm undoped BST (a), (c) and Mg doped BST (b), (d)

4.4 C-V measurement results:

The C-V characteristics of undoped and doped BST thin film of thickness 950nm annealed at 850^{0}C are given in figures 4.4.1 and 4.4.2 respectively.The capacitance of the thin film decreases with voltage. It is because of as increasing the bias electric field; the dramatic decrease in capacitance indicated the existence of symmetrical Schottky barriers. The dependence of the capacitance on the bias voltage shows a strongly nonlinear character. The interface capacitance formed by the Schottky barrier results its symmetry. It can be assumed that the SFM configuration behaves as a normal Schottky contact. The relationship of $1/C^2 \sim V$ or $1/\epsilon^2 \sim V$ can be employed to measure like semiconductor Schottky contact [50]. It can observed that Mg doped film has smaller value of capacitance and hence lower dielectric constant at zero bias voltage. It also support what we have found in XRD and FESEM results i.e. grain size of Mg doped thin film is smaller than undoped case and so lower value of dielectric constant is expected. A comparison of C – V characteristics of undoped and 5mol% Mg thin film is given in fig. 4.4.1.

The phenomenon of dispersion of dielectric permittivity may be attributed to extrinsic contributions to polarization of the materials such as impurities, oxygen vacancies, grain boundaries, domain wall motions [51]. It is well known that the value of the dielectric

constant of dielectric thin film is strongly affected by microstructure, grain structure, grain size [52] [53]. We think also, that in our case, the effect of the dopants is to decrease the polarization associated with the oxygen vacancies. The formation of non ferroelectric phases such as oxides can also largely decrease dielectric permittivity. However this smaller value of dielectric constant is favourable in perspective of our applications in microwaves as electrical tunable phase shifter [54].

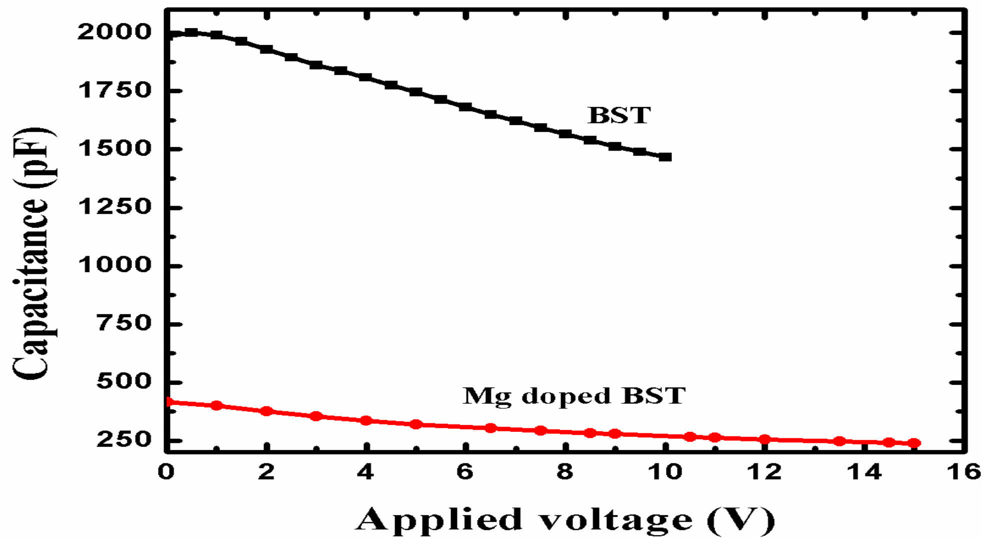

Figure 4.4 C vs. V for both undoped and 5mol% Mg doped BST thin film.

Figure 4.4.2 shows the variation of dielectric tunability defined as

$$\text{Tunability} = \varepsilon_{max.} - \varepsilon_{mim.}/\varepsilon_{max.} \qquad (4.1)$$

of the BST varactors with thickness. The dielectric tunability varies from 2 to 30 % when film thickness changes from 465 to 950 nm. Higher tunability can be achieved when the residual stress in the film is vastly relaxed as in the case of thick films. Meanwhile, the dielectric properties of a ferroelectric film are strongly influenced by grain size, grain structure, and quality of the material throughout the volume of the thin film. The dielectric tunability increases with grain size since the volume of dielectric polarization is propositional to the size of the grain [57, 58].

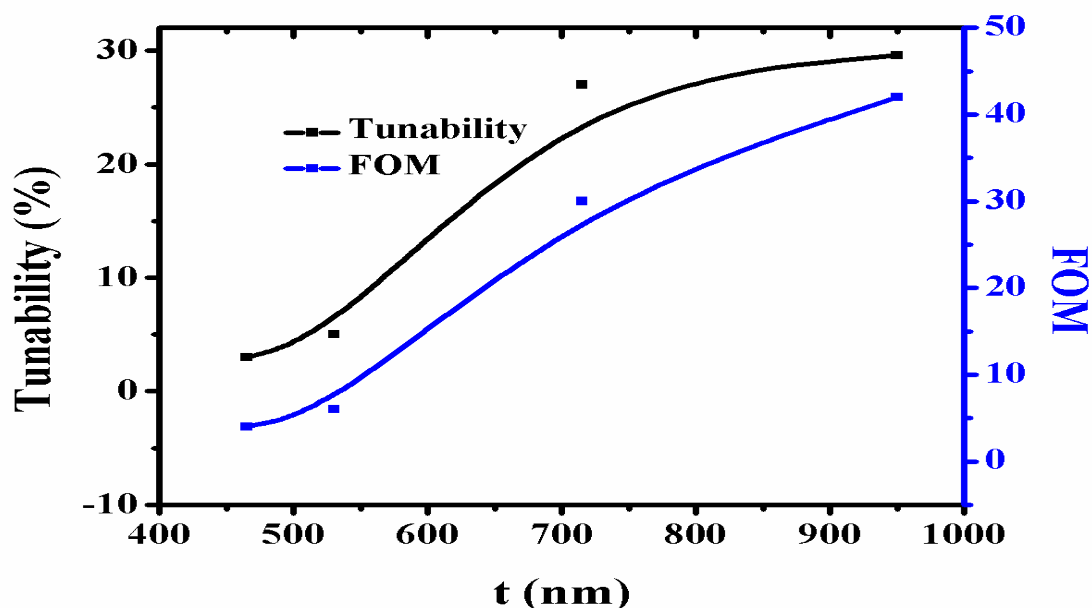

Figure 4.4.2 Variation of tunability and figure of merit (FOM) with film thickness

Thus, the increase of the tunability with increasing thickness is mainly due to increase in grain size and the strain relaxation. To fulfill the above, we need to optimize the processing conditions for a maximum value of the figure of merit (FOM) (defined as tunability/ loss). The Fig.4.4.2 shows the relationship between values of FOM and film thickness. It is interesting to note that the value of FOM shows a maximum for higher film thickness varactor.

4.5 Leakage current density measurement results:

Figure 4.5 shows the leakage current density variation with applied external field (J-E) for undoped and doped BST films. The electrical quality of a dielectric film is determined by the value of leakage current or resistivity of the ferroelectric thin films.

In the figure 4.5, it is clear that on increasing applied field leakage current density increase exponentially for both cases but Mg doped film has improve in leakage current density i.e. at bias field 80V/cm its value for undoped BST was 0.4 A/cm^2 and for doped case its value was 0.005 A/cm^2. The Mg-doped BST thin film possessed an enhanced film resistivity (low leakage current/high resistivity) value with respect to that of the undoped BST thin film.

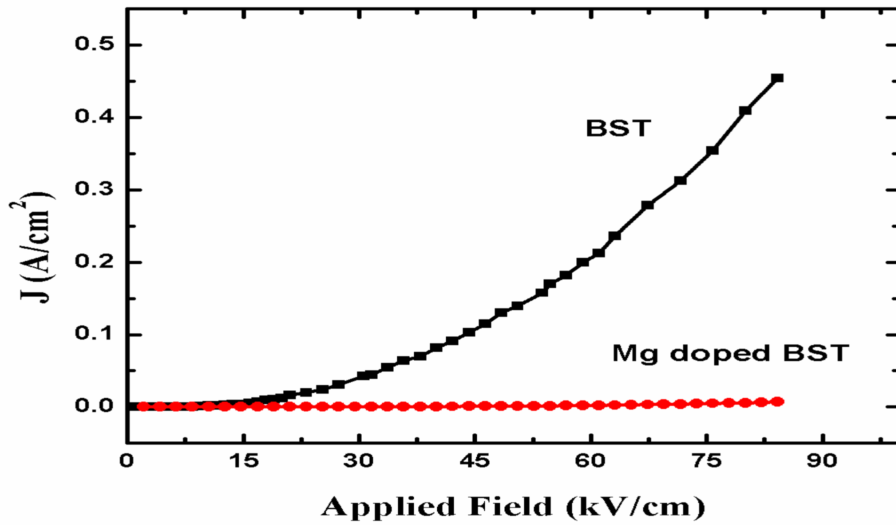

Figure 4.5 J vs. E for both undoped and 5mol% Mg doped BST thin film.

4.6 Loss tangent measurement results:

The loss tangent curves (fig. 4.6) may be explained by the presence of interfacial layers, such as surface electrode/film interface in the ferroelectric thin film [55, 56].The loss tangent is smaller for the doped film than that for the undoped ones. This can be related to the decrease of the oxygen vacancies in the doped film.

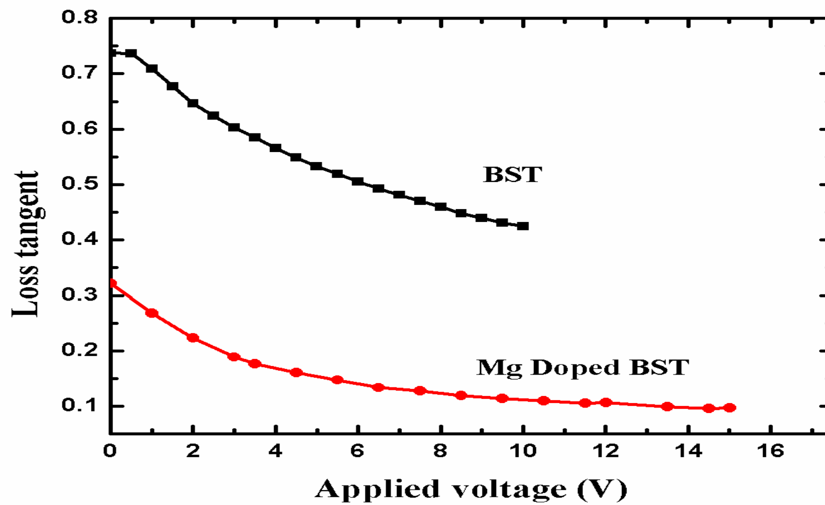

Figure 4.6 Loss tangent vs. applied voltage for both undoped and 5mol% Mg doped BST thin film.

It is because of acceptor type dopants can forbid the reduction of Ti^{4+} to Ti^{3+}, by neutralizing the donor action of the oxygen vacancies. Because the electrons resulting from the generation of oxygen vacancy can hop between different titanium ions and provide a mechanism for dielectric losses, the recompense for oxygen vacancy with the correct amount of acceptor dopants such as Mg^{2+}, should, help to lower the loss tangent. It is further speculated that Mg dopants serve to increase the insulation resistance (excellent film resistivity value) of the BST based film by suppressing the concentration of oxygen vacancies and growth of potential barrier at grain boundaries [57].

For example loss tangent value is 0.32 for doped case and 0.74 for the undoped case at zero bias conditions.

4.7 Quality factor (Q) measurement results:

Quality factor (Q) is defined as reciprocal of loss tangent i.e.

$$Q = 1/\text{(loss tangent)} = 1/\tan\delta \qquad (4.2)$$

The Q factor vs. bias voltage plots for undoped and doped BST thin film are shown in fig. 4.7. It is clear seen that quality factor increases with bias voltage.

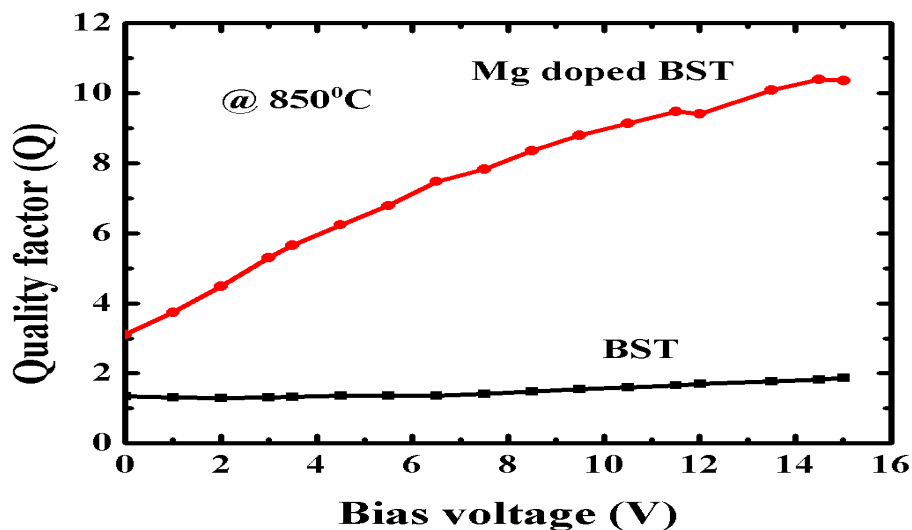

Figure 4.7.3 Q factor vs. applied voltage for both undoped and Mg doped BST thin film.

For Mg doped BST films Q is higher compared to undoped films. For example at 10V value of Q = 1.55 for undoped case and Q = 9 for Mg doped BST films, which shows remarkable impairment in doped films.

4.8 Return loss (S_{11}) measurement results:

Return loss of the thin film varactor is measured by “Rohde & Schwarz ZVL3 2Ports - Version 2.10” vector network analyzer having frequency range 900 kHz to 18 GHz. Return loss shows the amount of RF power reflected back from the thin film varactor in other word it indicate matching of the network i.e. if matching is good very less power will reflected back means maximum power will transmitted through thin film varactor. Figure 4.8.1shows the plots of S_{11} vs. frequency at zero volt and 30V bias for thin film varactor configuration.

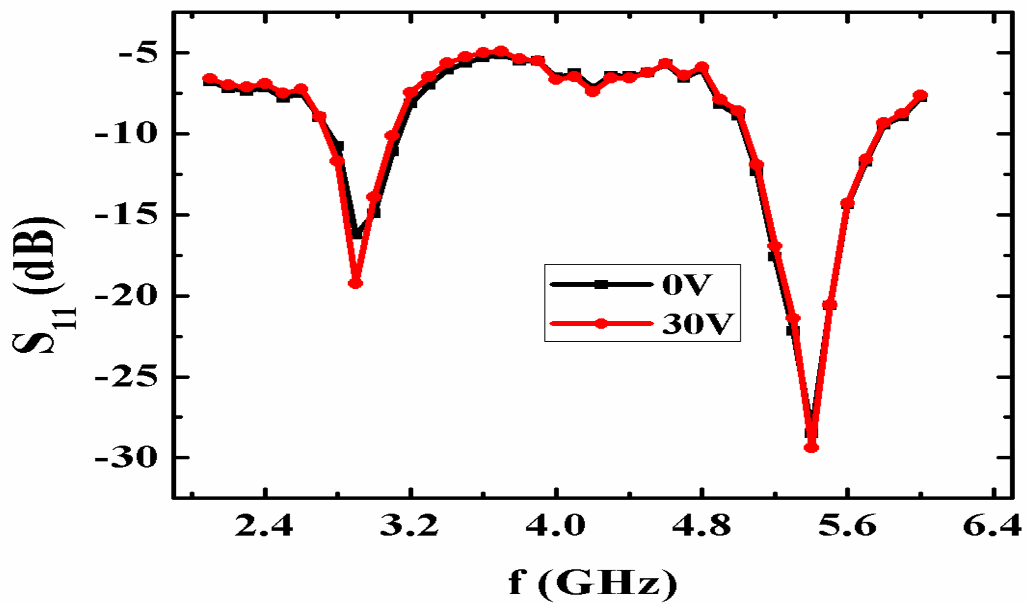

Figure 4.8.1 Measured return loss of coupled structure for undoped BST thin film.

The return loss for 0V and 30V bias volt with frequency shows that return loss is greater than 10dB for all biased voltage. It is clear that it has good performance in the frequency range of 2 GHz to 6 GHz because in this frequency range there are two dips in the curve which shows device performance will be good at these dips.

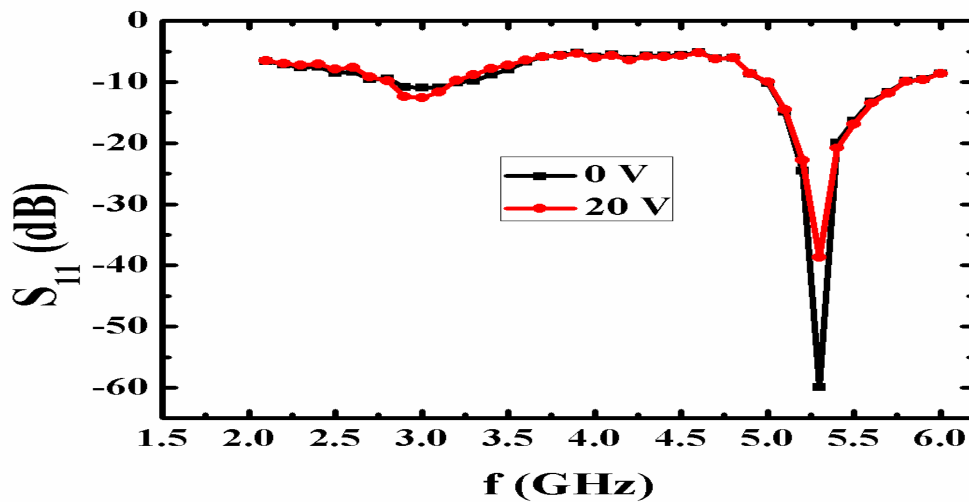

Figure 4.8.2 Measured return loss of coupled structure for 5mol% Mg doped BST thin film.

In case of 5mol% Mg doped (see fig. 4.8.2) return loss for 0V and 20V bias volt with frequency shows that return loss is greater than 10dB for all biased voltage. Figure 4.8.3 and 4.8.4 show S_{11} vs. bias voltage at fixed frequency of 2.9GHz. At zero bias the return loss S_{11} = 11dB which is lower than the undoped thin film varactor S_{11} = 17dB. At higher frequency of 5.3GHz S_{11} = 60dB for doped and S_{11} = 30dB for undoped case (see fig. 4.8.3 and 4.8.4)

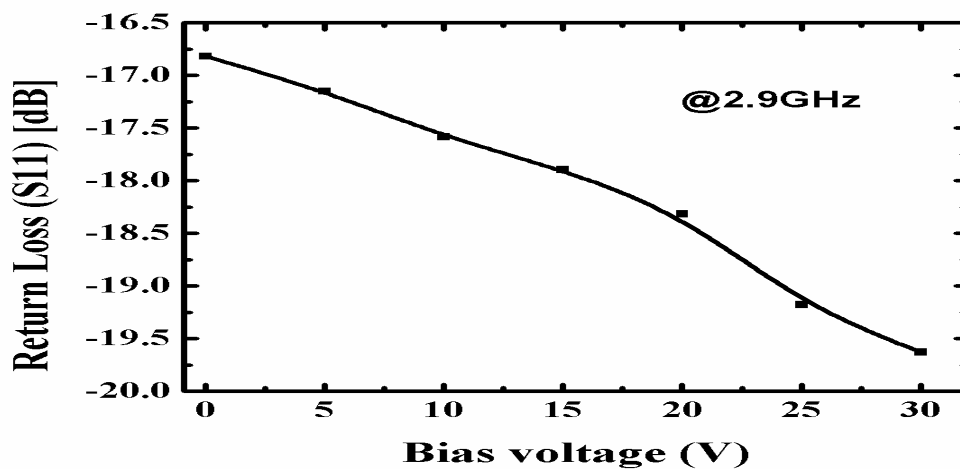

Figure 4.8.3 Measured return loss of coupled structure for undoped BST thin film with bias voltage.

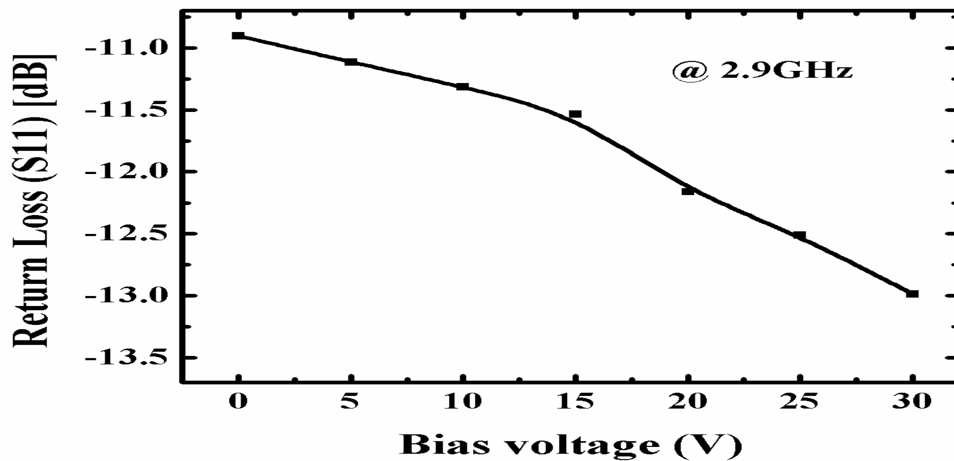

Figure 4.8.4 Measured return loss of coupled structure for 5mol% Mg doped BST thin film with bias voltage.

4.9 Phase shift measurement results:

The phase shift as a function of frequency was measured and the results are plotted in fig. 4.9.1 at two different bias voltages. It is the very important parameter for a phase shifter design. The measured return loss was better than 12dB from 2 GHz to 6 GHz. Therefore, the operating frequency of the phase shifter device was chosen in this frequency range. Figure 4.9.1 shows measured phase shift with respect to the zero bias state as a function of frequency under different bias voltages. A phase shift of 39 degree was obtained with a dc bias of 30 V at frequency of 5.4 GHz.

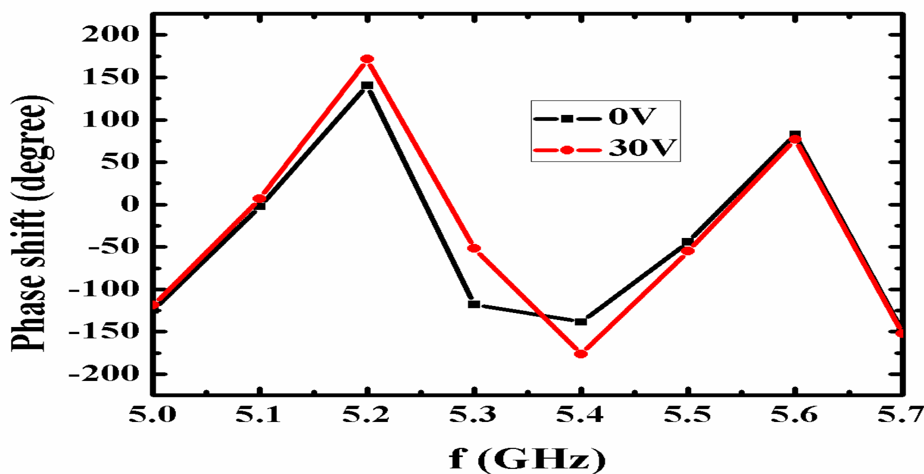

Figure 4.9.1 Differential phase shift of coupled structure for undoped BST thin film with frequency.

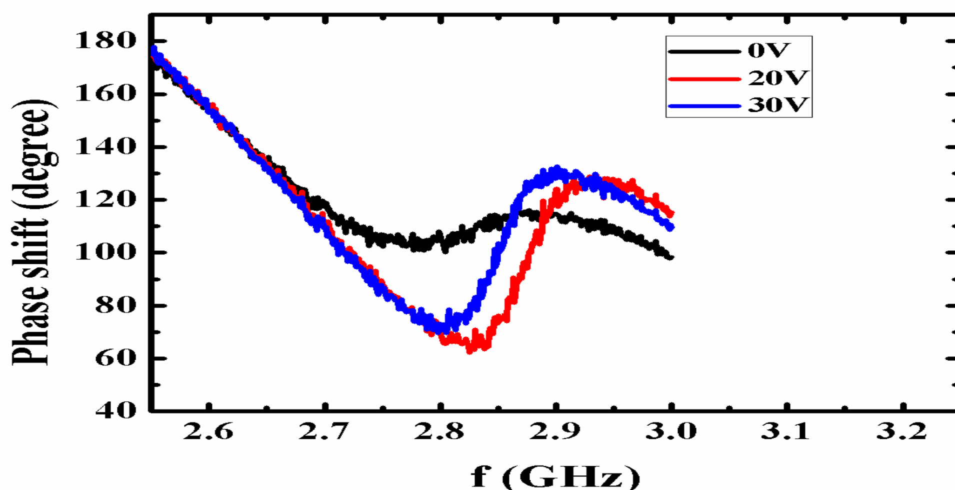

Figure 4.9.2 Differential phase shift of coupled structure for Mg doped BST thin film with frequency

Figure 4.9.2 shows measured differential phase shift with respect to the zero bias state as a function of frequency under different bias voltages. A phase shift of 34 degree was obtained with a dc bias of 30 V at frequency of 2.9 GHz.

Figure 4.9.3 shows measured differential phase shift with respect to the zero bias state as a function of bias voltage under different frequencies. A differential phase shift of 39 degree was obtained with a dc bias of 30 V at frequency of 2.9 GHz for undoped BST film and in case of Mg doped BST thin film its value was 34 degree at 2.9 GHz (see fig. 4.9.4).

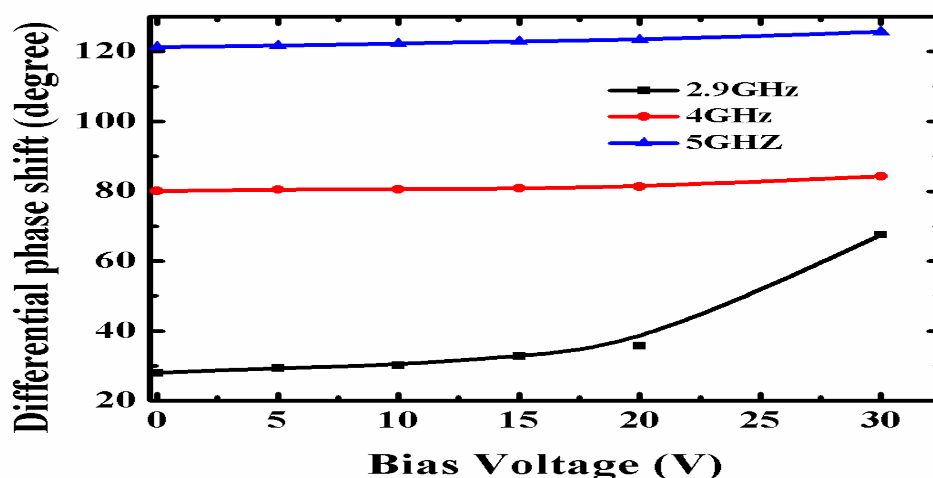

Figure 4.9.3 Differential phase shift of coupled structure for undoped BST thin film with bias voltage at different frequencies.

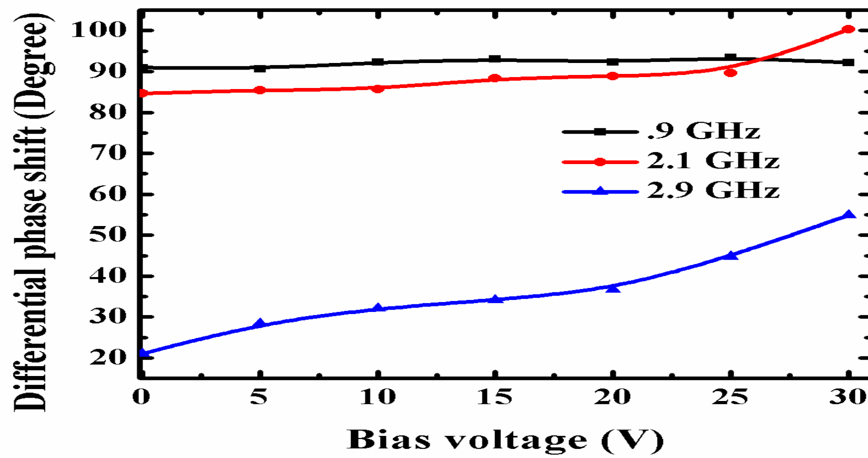

Figure 4.9.3 Differential phase shift of coupled structure for Mg doped BST thin film with bias voltage at different frequencies

4.10 Tunability and FOM measurement results:

Tunability of BST thin film varactor phase shifter is very important parameter. It shows change in phase shift per bias volt. Tunability is given by

$$\text{Tunability}\ (\%) = (\Delta\Phi/\Delta V) *100 \qquad (4.3)$$

The phase shift can be controlled by tuning of the transmission line. The first step in designing the varactor phase shifter is to determine the dimensions of each part of the coupled microstrip line to achieve the highest electrical tunability while maintaining the impedance matching. Electrical tunability of undoped and doped BST varactor is given in figure 4.10.1 and figure 4.10.2.

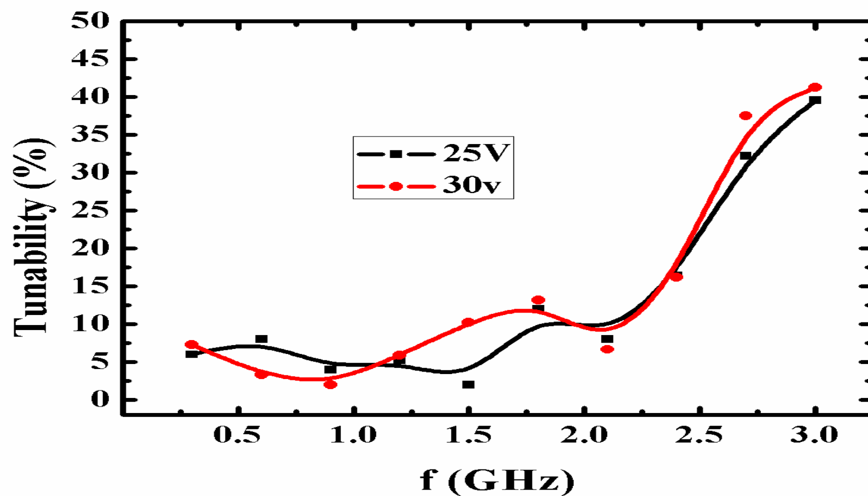

Figure 4.10.1 Tunability of coupled structure for undoped BST thin film with frequency at 25V and 30V bias voltage.

It is seen from figs.4.10.1 and 4.10.2 tunability in both cases varies nonlinearly with frequency. In case of pure BST its value is 41% where as for Mg doped BST its value is 39%.

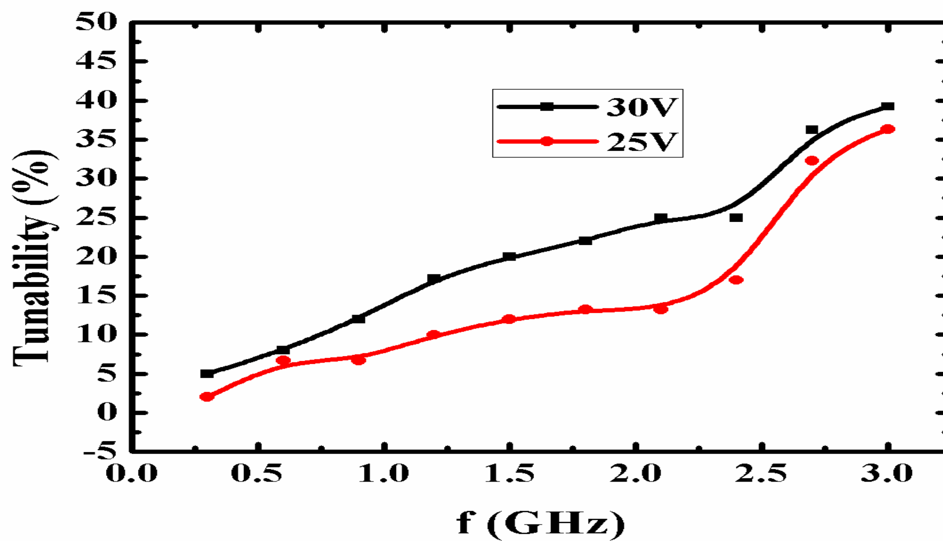

Figure 4.10.2 Tunability of coupled structure for doped BST thin film with frequency at 25V and 30V bias voltage.

For undoped BST varactor phase shifter differential phase shift was found to be 39 degree which corresponds to a figure of merit of ~15 degree /dB (see fig. 4.10.3) and in case of Mg doped its value was found to be ~21 degree /dB (see fig. 4.10.4). FOM defined as the maximum differential phase shift divided by the return loss averaged across the full voltage range. The figure of merit can be further improved by applying higher electric field, with the low bias voltages.

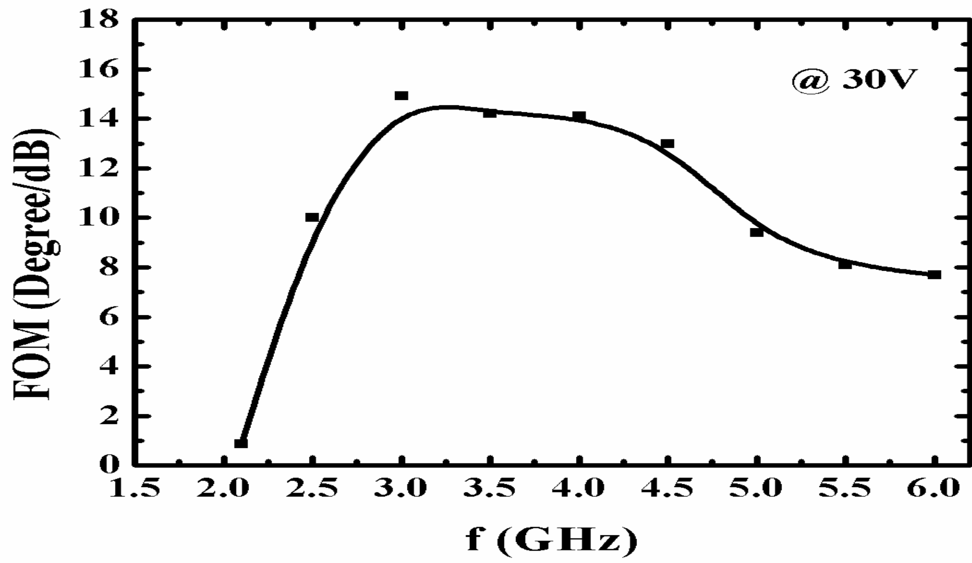

Figure 4.10.3 FOM for undoped BST thin film with frequency at 30V bias voltage.

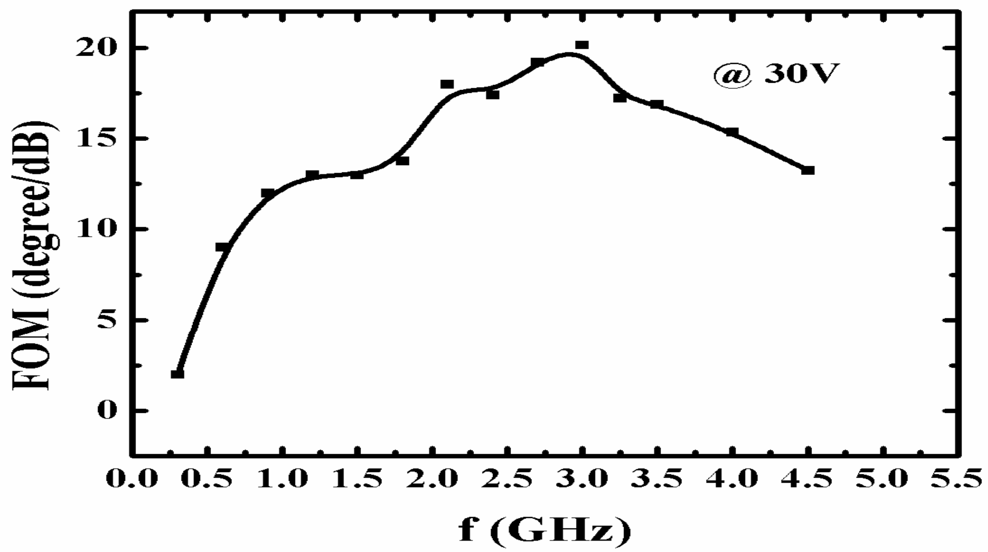

Figure 4.10.4 FOM for Mg doped BST thin film with frequency at 30V bias voltage.

CHAPTER 5

CONCLUSION AND FUTURE SCOPE

The BST thin films were fabricated by sol-gel based spin coating technique on single crystal n-type Si (100) substrate (resistivity ~7Ω-cm). The films of thickness 950nm annealed at 850^0C were dense, homogenous, crack-free and smooth with uniform thickness and uniform grain size. In addition the $Ba_xSr_{1-x}TiO_3$ (x=0.5) film showed no hysteresis in C –V characteristics indicating that the deposited films were paraelectric in nature for this composition.

The electrical characteristics of the thin films showed good dielectric and paraelectric properties. The measured leakage current density at 40 kV/cm is found to be 0.08 A/cm^2 and loss tangent = 0.7 at zero bias and 1MHz was obtained for undoped $Ba_xSr_{1-x}TiO_3$(x=0.5) thin film. In case of 5mol% Mg doped BST films the leakage current density is 0.0005A/cm^2 loss tangent was 0.3 at same conditions as used for pure BST films. The electrical properties of the BST thin films were found to be strongly dependent on thickness of BST film and growth temperature.

The maximum tunability ~ 41% in case of pure BST and ~39% in case of 5mol% Mg doped BST were found in the operational band from 2 GHz to 6 GHz and the measured return loss was better than 10 dB. A differential phase shift of 39^0 was obtained with a dc bias of 30 V at frequency of 2.9 GHz for pure BST and 34^0 in case of 5mol% Mg doped BST under same conditions. This will give the corresponding figure of merit of ~15°/dB for undoped BST and ~21^0/dB for the doped films. The phase shifter devices based on coupled microstrip line structure are less sensitive to interfacial effects and require simple processing. It can be concluded that Mg doped BST shows better dielectric properties than undoped BST, for example low loss tangent, less leakage current (was obtained for doped BST films), but with slightly lower tunability and figure of merit.

In future this newly proposed ferroelectric phase shifter and its equivalent circuit could also be used to find various microwave device applications using paraelectric materials.

REFERENCES

[1]. M. Di Domenico, D. A. Johnson, and R. H. Pantell, "*Ferroelectric garmonic generator and the large-signal microwave characteristics of ferroelectric ceramic*", *JAP.*, **33**(5), 1697-1706 (1962).

[2]. K. M. Johnson, "Variation *of dielectric constant with voltage in ferroelectric ceramics*", *JAP*, **33**(9), 2826-2831 (1962).

[3]. Yu. M. Poplavko, "*Ferroelectric with controlled dielectric permittivity in a waveguide*", *Radio Engineering*. **18** (10), 22-27 (1963).

[4]. S. N. Das, "*Quality of a ferroelectric material*", *IEEE Trans. MTT*, **12**(7), 440-445 (1964).

[5]. P. S. Neelakanta, "*Handbook of electromagnetic material: Monolithic and composite versions and their applications*", CRC press, 1995 pp279-291.

[6].Sheng Su, *"Tunable ferroelectric thin film devices for microwave applications",*NUS - 2011

[7]. O. G. Vendik, A.E. K. Hollmann, A. B. Kozyrev, and A. M. Prudan, *"Ferroelectric Tuning of Planar and Bulk Microwave Devices",* Supercond. Sci. Technol., 12(2), 325-338 (1999).

[8]. J.F. White, *"High power p-I-n diode controlled, microwave transmission phase shifters",IEEE Trans. Microwave Theory Tech.*, **13**, 233-242 (1965).

[9]. K. M. Johnson*, "Microwave varactor tuned transistor oscillator design"*, IEEE Trans. Microwave Theory Tech., 14, 564-572 (1966).

[10]. L. Lin, C. Nguyen, A.P. Pisano and R.T. Howe, *"Micro electromechanical filters for signal processing",* Proceedings of IEEE MEMS, MEMS '92, pp. 226-231(1992).

[11]. G. Rebeiz, *"RF MEMS Theory, Design, and Technology"*, Wiley, 2003.

[12]. Robert R. Romanofsky, Array Phase Shifters: Theory and Technology, NASA Technical Memorandum TM-2007-214906 (2007)

[13]. Eric Marsan, Jules Gauthier, Mohamed Chaker and Ke Wu, Tunable microwave device: status and perspective, IEEE-NEWCAS Conference, 2005. The 3rd International, Pages 279-283 (2005)

[14]. F. Reggia and E.G. Spencer, "A new technique in ferrite phase shifting for beam scanning of microwave antennas", Proc. IRE, 45, 1510-1517 (1957).

[15]. Gerald F. Dionne and Daniel E. Oates, "*Tunability of Microstrip Ferrite Resonator in the Partially Magnetized State",*IEEE trans. Magn.,33, 3421-3423 (1997).

[16]. Hong-Cheng Li, Weidong Si. et al. Oxide thin films for tunable microwave devices, Journal of Electroceramics, Volume 4 , issue 2/3, Pages 393-405 (2000)

[17]. O. G. Vendik, E. K. Hollmann, A. B. Kozyrev, and A. M. Prudan Ferroelectric tuning of planar and bulk microwave devices, Journal of Superconductivity, Volume12, Number 2, Pages 325-338 (1999)

[18]. Felix A Miranda, Fred W. VanKeuls, Robert R. Romanofsky, et al. Ferroelectric thin films-based technology for frequency- and phase- agile microwave communication applications, Integrated Ferroelectrics, Volume 42, Pages 131-149 (2002)

[19].A.K. Tagantsev, V.O. Sherman, K.F. Astafiev, J.V enkatesh, and N. Setter, Ferroelectric Materials for Microwave Tunable Applications, Journal of Electroceramics, Volume 11, Pages 5-66 (2003)

[20]. M J Lancaster, J Powell and A porch, *Thin-film ferroelectric microwave devices Superconductor Science and Technology,* Volume11, Nomber11, Pages1323-1334 (1998)

[21]. N. Setter, D. Damjanovic and L. Eng, Ferroelectric thin films: Review of materials, properties and applications, Journal of applied physics, 100, 051606 (2006)

[22]. M. W. Cole, C. Hubbard, E. Ngo, R. G. Geyer, M. Ervin, M. Wood, "Structure-property relationships in pure and acceptor-doped $Ba_{1-x}Sr_xTiO_3$ thin films for tunable microwave device applications",*JAP*. 92(1), 475-483 (2002).

[23]. S. Saha, S. B. Krupanidhi*, "Large reduction of leakage current by graded-layer La doping in BST thin films",APL* 79(1), 111-113 (2001).

[24]. T. G. In, S. Baik, S. Kim, "Leakage current of Al- or Nb-doped BST thin films by rf magnetron sputtering", J. Mater. Res.,13(4), 990-994 (1998).

[25]. Z. Yuan, Y. Lin, C.L. Chen, J. Weaver, X. Chen, *" Subramanyam G, Jiang J C, Meletis E I, Large dielectric tenability and microwave properties of Mn-doped (Ba,Sr)TiO_3 thin films"*, *APL* 87, 152901-1-3 (2005).

[26]. M. C. Chiu, H. C. Yao, C. J. Huang, F. S. shieu, *"Improvement of dielectric properties of $Ba_{0.6}Sr_{0.4}TiO_3$ thin films by MgO doping",JAP*., 102, 014110-1-8 (2007).

[27]. Q. X. Jia, B. H. Park, P. Lu, B. J. Gibbons, J. Y. Huang,*"Dielectric response and structural properties of TiO2-doped $Ba_{0.6}Sr_{0.4}TiO_3$ films", APL*., 81(1), 114-116 (2002).

[28]. M. W. Zhang, J. W. Zhai, X. Yao, *"Tunable and microwave dielectric properties of BST-BaWO4 composite ceramics doped with Co_2O_3",* Materials Research Bulletin, 45(12), 1990-1995 (2010).

[29]. D. W. Peng, J. R. Cheng, Z. Y. Meng, *"Low dielectric dissipation and enhanced tunability of $Ba_{0.6}Sr_{0.4}TiO_3$ thin films by the modified composition and multilayer structure",* Journal of Electroceramics, 21, 668-671 (2008).

[30]. W. F. Qin, J. Xiong, Y. R. Li, J. Zhu, J. L. Tang, W. J. Jie, Y. Zhang,*"Enhanced electrical properties of multilayer $Ba(Zr_{0.2}Ti_{0.8})O_3$/ $Ba_{0.6}Sr_{0.4}TiO_3$/$Ba(Zr_{0.2}Ti_{0.8})O_3$ thin films for tunable microwave applications"*, Journal of Materials Science, 43 (1), 409-412 (2008).

[31]. W. Fu, L. Cao, C.L. Choy, D. Wang, J. Miao, J. Qi, H. L. W. Chan,*"Dielectric properties Ba1.5Zn1.0Nb1.5O7/Mn-doped Ba0.6Sr0.4TiO3 hetero-layered films grown by pulsed laser deposition",*Appl. Phys. Lett., 89, 132908-1-3 (2006).

[32]. O. G. Vendik, *"Dielectric nonlinearity of the displacive ferroelectrics at UHF",*Ferroelectrics, Volume 12, Issue 1, Pages 85–90 (1976).

[33]. M J Lancaster, J Powell and A porch*, "Thin-film ferroelectric microwave devices Superconductor Science and Technology"*, Volume11, Nomber11, Pages1323-1334 (1998).

[34]. David S. Korn and Huey Daw Wu, *"A comprehensive review of microwave system requirements on thin-film, Integrated Ferroelectrics"*, Volume 24, Pages 215-237 (1999)

[35]. R. York, A. Nagra, E. Erker, J. Speck, T. Taylor, P. Periaswamy, S. Streiffer, and O. Auciello, *"Microwave Integrated Circuits using Thin-Film BST",*Applications of Ferroelectrics, 2000. ISAF2000. Proceedings of the 2000 12th IEEE International Symposium on, Volume 1, Pages 195-200 (2000).

[36]. P Bao, T J Jackson, X Wang and M J Lancaster, *"Barium strontium titanate thin film varactors for room-temperature microwave device applications"*,Journal of physics D: Applied physics, Volume 41, Number6, 063001, Pages1-21 (2008)

[37]. M J Lancaster, J Powell and A porch, Thin-film ferroelectric microwave devices Superconductor Science and Technology, Volume11, Nomber11, Pages1323-1334 (1998)

[38]. V. A. Vasiljev, K. A. Vorotilov, A.S. Sigov, M. I. Yanovskaya, L. I. Solovjeva,*"Sol-gel derived barium-strontium titanatefilms",*J. Sol-Gel Science Technol., 13, 877-883 (1998).

[39]. J. Yang, P.Yu, D. Q. Xiao, C. Tang, M. Chen*," The Fabrication of Highly (100)-Oriented Ba0.8Sr0.2TiO3/LaNiO3 Multilayer's via Sol-Gel Method"*, Ferroelectrics, 406, 90-96 (2010)

[40]. R.W. Schwartz, "Chemical solution deposition of perovskite thin films", Chem.Mater., Vol. 9, No. 11, pp. 2325-2340, 1997.

[41].E. Carlsson and S. Gevorgian, IEEE Trans. Microwave Theory Techn.47, 1544 (1999).

[42]. L. F. Chan, V.V. Vardan, C. K. Onga, C. P. Neo and V. K. Varadn, *"Microwave electronics: measurement and materials characterization",*John Wiley & Sons, Ltd, (2004).

[43]. R. A. York, *"TunableDielectrics for RF Circuits",* In: M. Steer, W. D. Plamer, eds., Multifunctional Adaptive Microwave Circuits and Systems. Scitech Publishing, (2009).

[44]. K. Ikuta, Y. Umeda, and Y. Ishii*," Upper-bound frequency for measuring mm-wave-band dielectric characteristics of thin films on semiconductor substrates"*,Jpn. J. Appl. Phys., 37, 210 (1998).

[45]. Y. Iwazaki, K. Ohta, T. Suzuki, *"Elimination of parasitic effects due to measurement conditions of $SrTiO_3$ thin films up to 40 GHz"*, J. European Ceramic Society, 26, 1841 (2006).

[46]. S. S. Gevorgian, T. Martinsson, P. L. J. linner, and E. L. Kollberg, *"CAD Models for Multilayered Substrate Interdigital Capacitors",* IEEE Transactions on Microwave Theory and Techniques, 44(6), 896 (1996).

[47]. S. W. Kirchoefer, A.C. Carter, K.K. Aga, J. M. Pond, W. Chang, K. K. Agarwal, J. S. Horwitz, and D. B. Chrisey, *"Microwave properties of BST thin-film interdigitated capacitors"*,Microwave Opt. Technol. Lett., 18(3), 168–171 (1998).

[48]. M.J. Lancaster, J. S. Hong,*"Microstrip Filters for RF/Microwave Applications"*,John Wiley & Sons, Inc.,(2001).

[49]. R.Garg, I. J. Bahl*, "Characteristics of coupled microstriplines"*, IEEE Trans. on MTT-27, 700-705 (1979). Corrections in IEEE Trans. on MTT-28, 272 (1980).

[50]. D. K. Schroeder, "*Semiconductor Material and Device Characterization"*Wiley-Interscience, New York, 1998_, Chap. 3, pp. 170–173.

[51]. J.H. Kim, Y. S. Yoon, D.L. Polla, Jpn. J. Appl. Phys. 37 (1998) 948- 950.

[52]. W. Hu, C. Yang and W. Zhang, Journal of Materials Science

[53]. X. Sun, B. Zhu, D. Wang, T. Liu, M. Li, X. Zhao, C. Sun, HLW. Chan, J ApplPhys 99 (2006) 084103

[54]. G. Vélu, K. Blary, J.C. Carru, G. Houzet, L. Burgnies, A. Marteau, D. Lippens, IEEE Microwave Theory and Techniques, vol. 55, n°2, 438, (2007).

[55]. S. B. Krupanidi and C. J. Peng, Thin Solid Films 305 (1997) 144

[56]. M. W. Cole, P. C. Joshi, and M. H. Ervin, J. Appl. Phys. 89 (2001) 6336.

[57]. M.W. Cole Novel, *"Tunable acceptor doped BST thin films for high quality tunable microwave devices",* Rev. Mex. F's. 50 (3) (2004) 232–238.

[58]. J. Pérez de la Cruz, E. Joanni, P. M. Vilarinho, and A. L. Kholkin, J. Appl. Phys. 108, 114106 (2010).

[59]. K. C. Sekhar, S.H. Key, J.Min, K. P. Hong, C. S. Han,Yook, D. S. Kim, J. C. Kim, J. C. Pak. Y. S. Cho, Curr. Appl. Phys.2, 654e658 (2012).